Elastic Light Scattering and Modulation from Solid Microspheres in Liquids

by

Huzeyfe Yılmaz

A Thesis Submitted to the
Graduate School of Sciences and Engineering
in Partial Fulfillment of the Requirements for
the Degree of

Master of Science

in

Physics

Koç University

August 2011

Koç University

Graduate School of Sciences and Engineering

This is to certify that I have examined this copy of a master's thesis by

Huzeyfe Yılmaz

and have found that it is complete and satisfactory in all respects,
and that any and all revisions required by the final
examining committee have been made.

Committee Members:

_____

Ali Serpengüzel, Ph. D. (Advisor)

_____

Alper Kiraz, Ph. D.

_____

Özgür Birer, Ph. D.

Date: _____

ABSTRACT

Optical microcavities have been extensively studied for the last few decades for their potential applications in lightwave communications and biochemical sensing. Among the different microcavity shapes and configurations studied so far, the microsphere is simplest resonator type due to the self-forming, ideal, and perfect nature of the sphere. For a sphere, the solutions to the electromagnetic fields subject to the boundary conditions, lead to the high quality factor optical resonances, which are strongly dependent on the morphology, i.e., size, shape and refractive index, of the spherical resonator.

In this work, solid dielectric and semiconductor microspheres are used as microresonators. The optical resonances of the microspheres are excited with tunable diode lasers through optical fiber half couplers. The observed transmission and the elastic scattering spectra reveal high quality factor optical resonances. The spheres are placed in various liquids, such as liquid crystals, organic liquids and aqueous solutions for the investigation of these optical resonances.

Nematic liquid crystals are highly birefringent molecules, which are vastly used in display technologies. Applying an external electric field to the nematic liquid crystal induces changes in the refractive index of the medium external to the microsphere. Hence the spectral position of the microspheres' optical resonances are tuned and used for signal modulation. This state-of-the-art microfluidic system promises novel optical signal processing applications in liquid crystal display and optofluidic technologies.

ÖZET

Optik mikroçınlaçlar üzerine, optik haberleşme ve biyokimyasal algılayıcı alanlarındaki olası uygulamaları nedeniyle son zamanlarda yoğun araştırmalar yapılmıştır. Yuvarın kendiliğinden oluşan, ülküsel ve kusursuz doğası nedeniyle mikroyuvarlar bütün optik mikroçınlaçlar arasında en temel olmuştur. Elektromanyetik alanların yuvarlak sınırlara uygulanarak çözülmesi sonucunda yüksek kalite faktörlü optik çınlamalar elde edilir. Optik çınlamaların özellikleri çınlacın yapısına (biçimine, boyutuna ve kırılma katsayısına) bağlıdır.

Bu çalışmada, mikroçınlaç olarak katı yalıtkan ve yarı iletken mikroyuvarlar seçilmiştir. Optik çınlamalar, izge ayarlı bir lazer ve fiber optik yarı bağlaştırıcı ile uyarılmıştır. Optik liften iletilen ve mikroyuvardan saçılan ışık izgeleri optik çınlamalar göstermiştir. Çınlamaların araştırılması için mikroyuvarlar sıvı kristal, organik sıvılar ve su çözeltileri gibi sıvılar içine yerleştirilmiştir.

Nematik fazlı sıvı kristaller yüksek derecede çift kırılma katsayılı, görüntüleme teknolojisinde çok kullanılan moleküllerdir. Mikroyuvarı çevreleyen nematik sıvı kristallere elektrik alan uygulanması mikroyuvarın etrafında kırılma katsayısının değişmesi gibi yapısal değişikliklere neden olur. Dolayısıyla optik çınlamaların izge konumu ayarlanabilir ve optik im kiplenebilir. Bu optoakışkan sistem sıvı kristalli görüntüleme teknolojilerinde ve optik im işlenmesi uygulamalarında yeni olanaklar sunmaktadır.

ACKNOWLEDGEMENTS

First of all I would like to thank my advisor Prof. Ali Serpengüzel for giving me the chance to work in Koç University Microphotonics Research Laboratory, for his guidance, kindness and generous help throughout my Master of Science Thesis research.

Then I would like to thank Assoc. Prof. Alper Kiraz and Asst. Prof. Özgür Birer for participating as committee members in my thesis and their valuable feedback.

I would also like to thank Koç University Microphotonics Research Laboratory members; Mohammed Sharif Murib, Ersin Hüseyinoğlu, Hasan Yılmaz, Ulaş Sabahattin Gökay, and Seyed Alireza Aleali for their help in the laboratory and for the discussions we had.

For their endless love and support, I would like to thank my parents and my brother, Erkam.

Finally, I would like to acknowledge Türkiye Bilimsel ve Teknolojik Araştırma Kurumu (TÜBİTAK) grant No. EEEAG - 106E215 for their financial support to our research.

TABLE OF CONTENTS

List of Figures

NOMENCLATURE

a	Radius of the microsphere
a_n	Transverse magnetic (TM) mode elastic scattering field coefficient
b_n	Transverse electric (TE) mode elastic scattering field coefficient
B	root mean square (RMS) size of inhomogeneities
$\vec{E}$	Electric field vector
F	Free energy of nematic liquid crystals
$F_{elastic}$	Elastic energy density of a deformed nematic liquid crystal cell
$h_n^1(x)$	Spherical Hankel function of the first kind
$j_n(x)$	Spherical Bessel function
K	Kerr coefficient
k	Wave vector, propagation vector, propagation constant
k_1	Splay deformation constant of the liquid crystal
k_2	Twist deformation constant of the liquid crystal
k_3	Bend deformation constant of the liquid crystal
l	Radial mode order of the MDR
m	Angular mode number of the MDR
M	Relative refractive index of the microsphere
n	Polar angular mode number of the MDR
N_1	Refractive index of the microsphere
N	Refractive index of the medium
N_e	Extraordinary refractive index
N_o	Ordinary refractive index
$\hat{n}$	Director vector of the liquid crystal
Q	Quality factor of the MDR

Q_{abs}	Quality factor associated with the absorption losses
Q_{con}	Quality factor associated with the surface contaminants
Q_{ext}	Quality factor associated with the coupling losses
Q_{rad}	Quality factor associated with the radiation losses
$Q_{s.s}$	Quality factor associated with the scattering losses
P	Power stored in a cavity
P_n^m	Legendre polynomials of the first kind of order m, degree n
S	Orientational order parameter
T	Period of a photon
t	Transmission coefficient through the optical fiber
U	Electrostatic energy of nematic liquid crystals
W	Energy stored in a cavity
$\Delta w_{1/2}$	Full width at half maximum in angular frequency
x	Size parameter of the microsphere
z_n	Any one of the four spherical Bessel function
α	Attenuation of optical power in a material
α_{ex}	Excess polarizability
$\Delta\lambda$	Mode spacing in wavelength
$\Delta\lambda_{1/2}$	Full-width-at-half-maximum (FWHM) in wavelength
ε	Permittivity of the medium
$\underline{\underline{\varepsilon}}$	Permittivity parallel to director axis
$\varepsilon_{\perp}$	Permittivity perpendicular to director axis
λ	Wavelength of light in vacuum
ξ	Riccati-Bessel function for the spherical Hankel Function of the first kind
σ_s	Surface density of particles
ψ_{emn}	Characteristic spherical wave equation
ψ_n	Riccati-Bessel function for the spherical Bessel function

Chapter 1

INTRODUCTION

Nowadays, liquid crystal displays (LCD's) are all around us, from cell phones to televisions and computer screens. At first LCD's were only used in digital watches and calculators, however at the moment, LCD's have replaced cathode ray tubes (CRT's) and even have created novel application areas such as notebooks and cell phones. Since the invention of the thin film transistor (TFT) array display, the need for better optical signal processing and demand for higher resolution in LCD's has been increasing in the display industry [1].

On the other hand, the last few decades witnessed an increase in the use of optical microcavities for their high light confinement in very small mode volumes and ultrahigh quality factor modes [2]. The pursuit of high speed signal processing led to the development of optical circuits instead of electronic circuits. Since then, optical microcavities have been serving as building blocks for photonics [3, 4]. Applications in new light sources, cavity quantum electrodynamics [6], semiconductor quantum well structures and optical communications such as switching and filtering [7], ultrafast modulation [8] and wavelength tuning [9] make optical microcavities essential tools for photonics. Fabry-Perot, whispering gallery and photonic crystal microcavities are the three types of microcavities for the method of light confinement [10]. Whispering gallery mode microcavities are so called, because of the analogous sound wave confinement in acoustic structures. Another appropriate term for optical resonances inside a spherical microcavity is Morphology Dependent Resonances (MDR's).

Sphere is one of the simplest geometry found in nature. MDR's of a spherical resonator are well defined with the help of the wave nature of light. However the dependencies on

polar, radial and azimuthal fields make the treatment of the resonances of a microsphere very complicated. Beside easy fabrication and self forming properties, microspheres can sustain resonances with narrow linewidths due to the very low optical loss inside the resonator [11]. Among all the microcavities, the highest quality factors are achieved with microspheres. High quality factor resonators are necessary in numerous applications. Recently, microspheres have been used for nanoparticle and protein detection [12]. In this work, a novel application for microspheres as optical microcavities is proposed for combining the birefringence and the electro-optic effects of nematic liquid crystals (NLC's) with optical resonances of microspheres. This combination opens the door to brand new ideas and applications for LCD's.

Chapter 2 starts with the basic understanding of optical resonances within a spherical microcavity. Before getting into the solutions of the electromagnetic fields with spherical boundary conditions, the underlying concept of resonance is illustrated with the help of geometric optics. Later, solutions of electromagnetic fields and general properties of resonances are stated. In the end, the experimental methods for exciting the resonances, the critical conditions and parameters for efficient excitation are described.

Chapter 3 focuses on the exercises and applications of MDR's. The shift of resonances, effects and mechanisms responsible for shifts and related applications are presented.

Experimental setups and related results are presented in chapter 4. MDR's of dielectric and semiconductor microspheres in air, water, ethylene glycol, and liquid crystal are investigated. The setups built for the excitation of resonances are demonstrated. Methods to use NLC's with fused silica optical fiber couplers and semiconductor microspheres and the results are presented.

Finally, the thesis is concluded with the summary of the work done and discussion of results. Suggestions for future work are submitted.

Chapter 2

SPHERICAL MICROCAVITIES

2.1. Introduction

Let us consider a light beam incident on the surface of a spherical cavity with the angle of incidence higher than that of the critical value ($\theta_{incident} > \theta_{critical} = arcsin(N/N_1)$) where, a is the radius of the spherical cavity, N_1 the refractive index of the cavity material, N the refractive index of the medium, and $M = N_1/N$ is the relative refractive index. Due to the spherical symmetry, light rays reflected from the inner surface of the cavity have the same incident angle for every reflection, so that total internal reflection (TIR) is achieved.

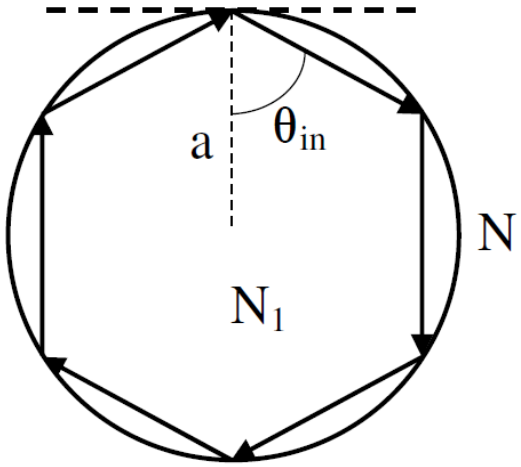

Figure 2.1. Propagation of light with TIR. θ_{in} is the angle of incidence.

Then, the following equations and the explanations define the morphology dependent resonances (MDR's). Whenever the incident light, with wavelength λ in vacuum, is in phase with the reflected light, a standing wave occurs in the cavity. For large microcavities *($a \gg \lambda$)*, the standing wave is close to the surface. Hence the distance that the wave travels

in one round trip is approximately equal to the circumference of the sphere. Then, for a microsphere with refractive index N_1 and radius a, the condition for the standing wave to occur is

$$n\frac{\lambda}{N_1} \approx 2\pi a \tag{2.1},$$

where λ/N_1 is the wavelength in the microsphere and n an integer. Frequently, a dimensionless size parameter x is defined to be used in expressions of this system

$$x = ka = \frac{2\pi Na}{\lambda} \tag{2.2}.$$

where k is the propagation vector in the surrounding medium. The standing wave condition can then be expressed as

$$x \approx \frac{nN}{N_1} = \frac{n}{M} \tag{2.3}.$$

Equation 2.3 shows that the standing wave or the so called MDR's are dependent on a quantum number n, on the size of the microsphere, and the refractive index of the medium and the microsphere. However, equation 2.3 is obtained with the geometric interpretation and for further analysis the electromagnetic problem, the Helmholtz equation with spherical boundary conditions has to be solved [4].

2.2. Morphology Dependent Resonances

In order to understand the characteristics of the morphology dependent resonances, the electromagnetic problem has to be solved. The solutions to the Helmholtz Equation for spherical boundary conditions were obtained by Mie first in the 19th century [5]. Attaining the solutions for the electromagnetic problem requires a rigorous derivation. In this thesis, only key equations will be highlighted for a brief introduction.

Let us consider a plane wave for the excitation of resonances. In this context, notations for spherical coordinates will be used. A plane wave can be expanded in terms of vector spherical harmonics. The characteristic equations that satisfy the scalar wave equation in spherical polar coordinates are then,

$$\psi_{emn} = \cos(m\phi)P_n^m(\cos\theta)z_n(kr) \ , \qquad (2.6a),$$

$$\psi_{omn} = \sin(m\phi)P_n^m(\cos\theta)z_n(kr) , \qquad (2.6b),$$

where $P_n^m(\cos\theta)$ is the Legendre polynomials of the first kind of degree *n* and order *m* and $z_n(kr)$ represents any of the four spherical Bessel functions. Hence the vector spherical harmonics expansion of a plane wave is,

$$\vec{E}_i = E_0 \sum_{n=1}^{\infty} i^n \frac{2n+1}{n(n+1)} (\vec{M}_{o1n}^{(1)} - i\vec{N}_{e1n}^{(1)}) \ , \qquad (2.7),$$

where $\vec{M}_{o1n}^{(1)} = \vec{\nabla} \times (\vec{r}\psi_{o1n})$ and $\vec{N}_{e1n}^{(1)} = \frac{\vec{\nabla} \times \vec{M}_{e1n}^{(1)}}{k}$ [13,14]. For a homogeneous, isotropic microsphere with radius a, the scattered electric field is then expressed as

$$\vec{E} = \sum_{n=1}^{\infty} E_n (a_n i\vec{N}_{e1n}^{(3)} - b_n \vec{M}_{o1n}^{(3)}) . \quad (2.8).$$

The elastic scattering coefficients, a_n and b_n, can be simplified by the help of the Riccati-Bessel functions,

$$\psi_n(r) = rj_n(r) \text{ and } \xi(r) = rh_n^{(1)}(r), \quad (2.9),$$

where $j_n(z)$ and $h_n^1(z)$ are the spherical Bessel function and the spherical Hankel function of the first kind, respectively. Finally a_n and b_n can be expressed as

$$a_n = \frac{\psi_n'(Mx)\psi_n(x) - M\psi_n'(x)\psi_n(Mx)}{\psi_n'(Mx)\xi_n(x) - M\psi_n(Mx)\xi_n'(x)} \quad (2.10).$$

and

$$b_n = \frac{M\psi_n'(Mx)\psi_n(x) - \psi_n'(x)\psi_n(Mx)}{M\psi_n'(Mx)\xi_n(x) - \psi_n(Mx)\xi_n'(x)} \quad (2.11).$$

Note that, equations 2.10 and 2.11 are obtained for a plane wave excitation of MDR's. However, for most of the applications guided waves are used, hence the profile of the input light beam has to be introduced into the elastic scattering coefficients. Nevertheless, the denominators of the scattering coefficients will not change, because the resonances occur at the poles, and are defined with the size parameter, *x*, and the relative refractive index, m [15, 16]. Moreover, there are two scattering coefficients which correspond to the two classes of solutions. One of which is for transverse electric (TE) modes because of the absence of electric field in the direction of propagation of the electromagnetic field in the microsphere. Transverse magnetic (TM) modes are defined in the same sense. Along the

microsphere circumference, where the resonant field stands in, TM modes have electric field components. As a result, electric fields of TM modes posses a more radial character.

From here on, the characteristic equations can be deduced and the solutions with energies in the range of the potential well correspond to the optical resonances in a dielectric microsphere. The two classes of solutions for TE and TM modes are analogous to the quantized energy levels of the quantum mechanical problem. MDR's are associated with polar mode number (*n*), radial mode number (*l*), and azimuthal mode number (*m*). The spherical symmetry induces degeneracy in the azimuthal modes. For each polar mode number *n,* there are *2n+1* azimuthal modes.

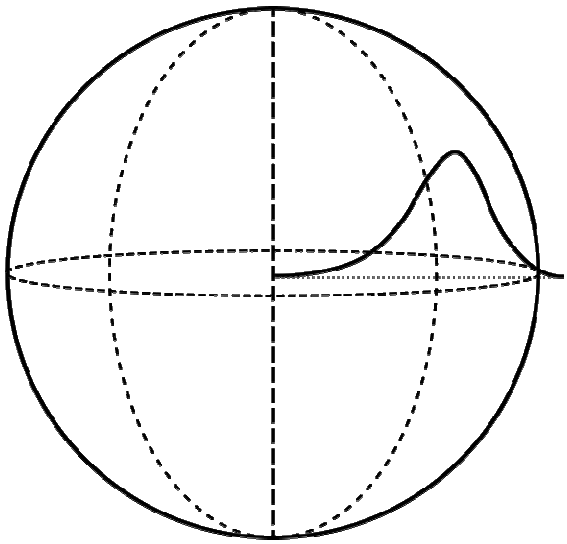

Figure 2.2. Representative radial field distribution of resonances in a microsphere.

2.2.1 Properties of MDR's

In electronics, quality factor, Q factor, is used as a parameter to define how under-damped an oscillation or a resonance is [19]. Also the bandwidth of a resonance is related to the Q factor [20]. A more general definition for the Q factor is the caliber for the quality

of a resonance. For an optical resonator, quality factor is the ratio of the energy stored in the fields to the energy lost per cycle,

$$Q = \frac{2\pi W}{PT} \tag{2.12},$$

where W is the stored energy, $P = -dW/dt$ the power dissipation, $T = 2\pi/w_0$ the period and w_o the resonant frequency [21]. Then the Q factor becomes

$$Q = -\frac{w_0 W}{dW/dt}. \tag{2.13}.$$

Also the energy stored as a function of time can be expressed in terms of the Q factor,

$$W(t) = W_o \exp(\frac{-w_0 t}{Q}). \tag{2.14}.$$

Now, the Q factor can also be a parameter to define the average lifetime of a photon in the resonant mode, $\tau = Q/w_0$. Furthermore, the number of cycles for the energy stored to decrease to $e^{-\pi}$ times of its original value is Q [22]. The electric field in a cavity varies as

$$E(t) = E_o \exp(iw_0 t)\exp(-w_0 t/Q). \tag{2.15}.$$

Then the energy in the cavity near a resonant frequency becomes,

$$|E(w)|^2 \propto \frac{1}{(w-w_0)^2 + (\frac{w_0}{2Q})^2} \quad . \qquad (2.16).$$

The resonance intensity has a Lorentzian lineshape. Q factor is measured from a resonance as its full-width-at-half-maximum (FWHM) of its energy value. At the half maximum energy of a resonant field, $|w - w_0| = w_0/2Q$. The quality factor then, can be measured from the Lorentzian resonances since,

$$Q = \frac{w_0}{\Delta w_{1/2}} \quad \text{or} \quad Q = \frac{\lambda_0}{\Delta \lambda_{1/2}} \qquad (2.17).$$

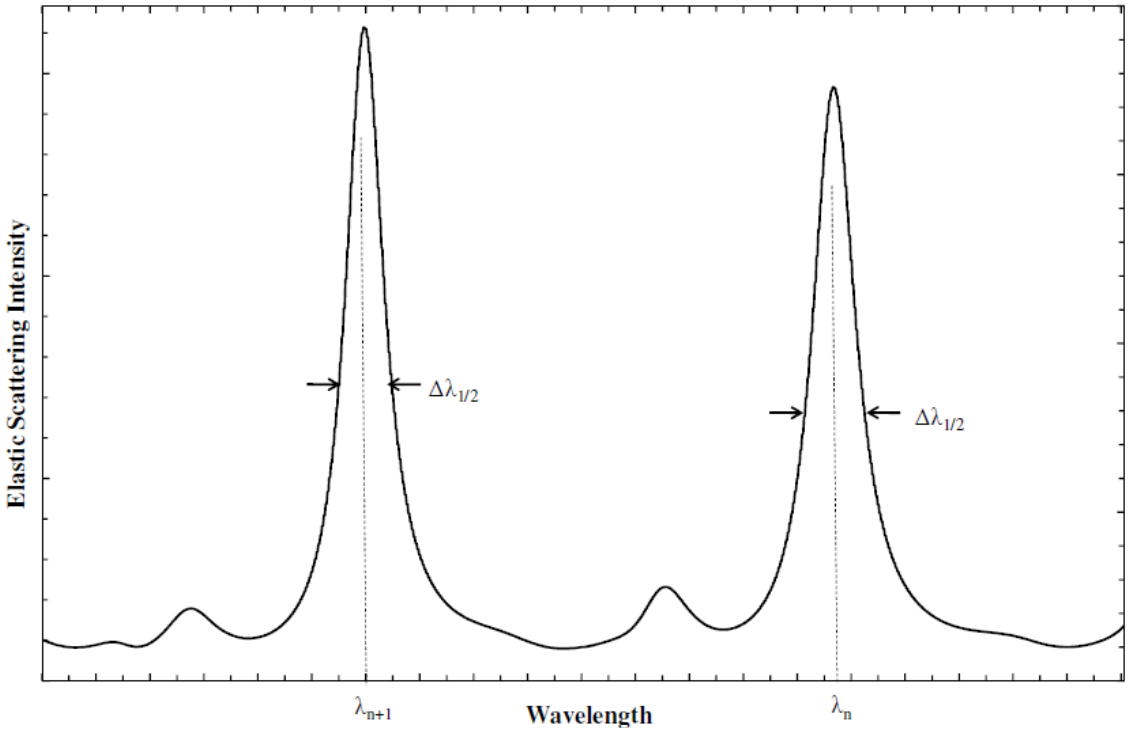

Figure 2.3.Representative linewidths for resonances.

A microsphere is a dissipative cavity because of the loss mechanisms such as radiative losses, material absorption, scattering losses and surface contaminant losses. Consequently,

$$Q_{total}^{-1} = Q_{rad}^{-1} + Q_{abs}^{-1} + Q_{s.s}^{-1} + Q_{con}^{-1} + Q_{ext}^{-1} \quad (2.18).$$

Q_{rad}^{-1} stands for the radiative losses. Radiative losses are caused by the imperfect nature of the total internal reflection (TIR) from a curved surface. Evanescent field on the surface of the resonator becomes propagating and the photons tunnel out of their bound states. The radiative losses can be expressed with a semiclassical approximation

$$Q_{rad} \cong xe^{2(l+1/2)g(\frac{x}{l+1/2})} \quad (2.19),$$

where $g(y) = -\sqrt{1-y^2} + \arg\cosh(1/y)$, x the size parameter, and l the radial mode number [11]. Radiative losses are also referred to as whispering gallery losses and treated in a similar manner for an approximate analytic formula [23]. If highly confined modes are considered, radiative losses become less dominant and even negligible, when compared to the absorption losses.

Q_{mat}^{-1} represents the material absorption and bulk Rayleigh scattering losses. α being the attenuation coefficient of the material in units of *dB/km*,

$$Q_{mat} \cong \frac{4.3\times10^3}{\alpha}\frac{2\pi N}{\lambda} \quad (2.20),$$

is the approximation for the intrinsic material loss in a microsphere [11].

$Q_{s.s}^{-1}$ indicates the scattering losses caused by the remaining surface inhomogeneities. Estimated scattering losses are dependent on the rms size (σ) and the correlation length (B) of the inhomogeneities [24],

$$Q_{s.s} = \frac{\lambda^2 a}{\pi^2 \sigma^2 B} \tag{2.21}.$$

Note that, as the sphere radius (*a*) increases, $Q_{s.s}$ gets bigger. Hence Q factors exceeding 10^{10} can only be expected in microspheres with diameters larger than 100 μm [25].

Q_{cont}^{-1} denotes the losses due to the surface contaminants resultant from the fabrication process. In silica microspheres, it has been shown that, water contamination on the surface of the microspheres limit the ultimate quality factor [24].

Finally, Q_{ext}^{-1} is the external coupling losses from the microsphere resonator to the modes of a waveguide or a prism.

Another important feature of a morphology dependent resonance (MDR) is the mode spacing or the free spectral range (FSR). FSR is the term, that describes the spacing in optical wavelength (or frequency) between two transmitted (or scattered) optical maxima [26]. However, the term FSR is originated for Fabry-Perot interferometers. As mentioned before in this thesis, a spherical microcavity can support very complicated resonances. Hence, the spacing between two successive modes (or resonances) has to be associated with the mode (or the resonance). Although, FSR is a more familiar term and is used sometimes for spherical optical microcavities, mode spacing is a better term in depicting the spectral signature of the microsphere. Mode spacing was first derived for the size parameter and is defined as the spacing between two successful polar modes *n* and *n+1* having the same radial mode number *l*. Hence the size parameter distance between

successive modes is $\Delta x_n = x_{n+1} - x_n$ where n is the polar mode number. The size parameter mode spacing is given as

$$\Delta x = \frac{x \arctan\left[\left(\left(\frac{Mx}{n}\right)^2 - 1\right)^{1/2}\right]}{n\left(\left(\frac{Mx}{n}\right)^2 - 1\right)^{1/2}} \qquad (2.22).$$

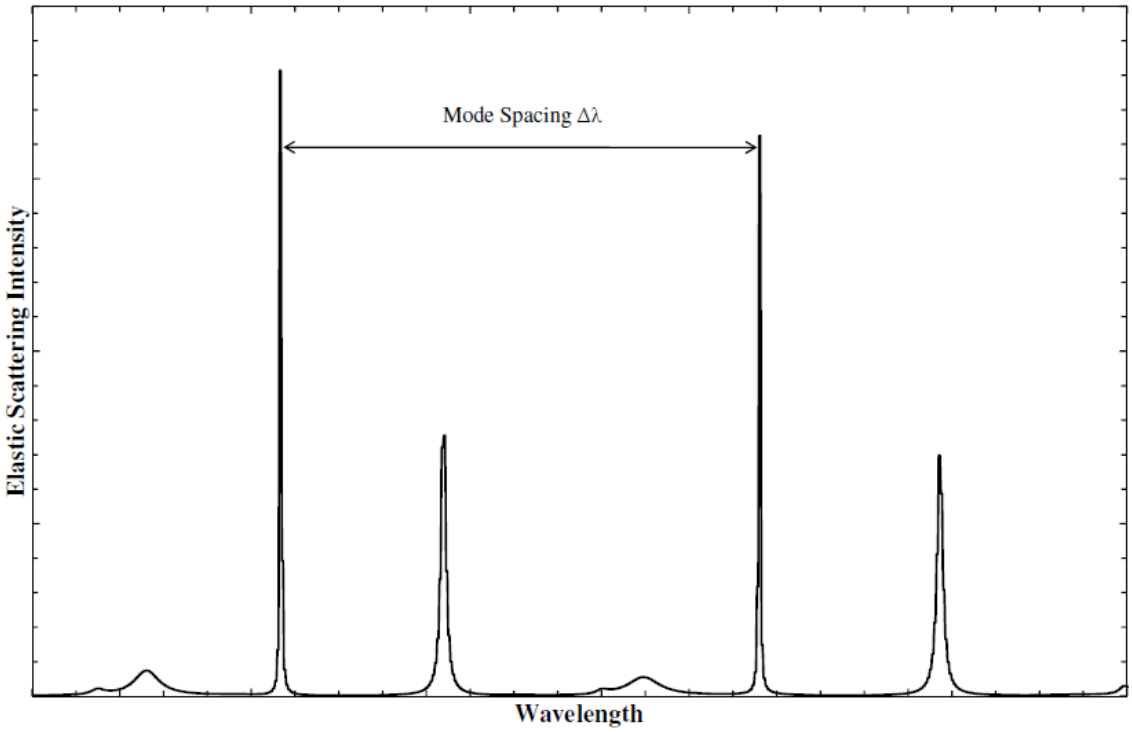

Figure 2.4.Representative mode spacing for resonances.

Recall that size parameter is defined as $x = 2\pi Na/\lambda$ and N is the relative refractive index of the medium. Therefore, $x_{n+1} = 2\pi Na/\lambda_{n+1}$ and $x_n = 2\,\pi Na/\lambda_n$. Then size parameter spacing can be expressed in terms of the wavelength spacing for successive modes,

$$\Delta x = \frac{2\pi Na(\Delta\lambda)}{\lambda^2} \tag{2.23},$$

where $\lambda^2 = \lambda_{n+1}\,\lambda_n$ and $\Delta\lambda = \lambda_{n+1} - \lambda_n$. Equation 2.22 can now be expressed for wavelength spacing,

$$\Delta\lambda = \frac{\lambda \arctan\left[\left(\left(\frac{Mx}{n}\right)^2 - 1\right)^{1/2}\right]}{n\left(\left(\frac{Mx}{n}\right)^2 - 1\right)^{1/2}} \tag{2.24}.$$

When the size parameter and the polar mode number are much larger than 1 ($x >> 1$ and $n >> 1$), and when their ratio is close to 1 ($x/n \sim 1$) equation 2.22 can be simplified into

$$\Delta x = \frac{\arctan\left[(M^2-1)^{1/2}\right]}{(M^2-1)^{1/2}} \tag{2.25}.$$

Again equation 2.25 can be rewritten as the mode spacing for wavelength using equation 2.23,

$$\Delta\lambda = \frac{\lambda^2 \arctan\left[(M^2-1)^{1/2}\right]}{2\pi aN(M^2-1)^{1/2}} \tag{2.26}.$$

Equations 2.24 and 2.26 can predict the mode spacing accurately. The conditions for using equation 2.26 and 2.25 are explained above. When, $x/n \sim 1$ is not satisfied and $|x-n| >> 1/2$ equation 2.24 and 2.22 should be used instead. In fact, when $|x-n| \geq 4$ is satisfied, Equation 2.24 can predict the mode spacing with 1% accuracy and in the case of $|x-n| < 4$, equation 2.26 can determine the resonance mode spacing with the same accuracy [27, 28].

2.3 Excitation of MDR's

The complete capability and future of microspheres can be unfolded with adequate observation of MDR's. Therefore the excitation of MDR's becomes the most crucial step. Excitation of MDR's is entirely related to coupling light into the spherical microcavity. For applications and research with microspheres; robust, efficient and controllable coupling is essential. Phase matched evanescent field coupling is the only approach that meets these critical requirements.

2.3.1 Coupling Analysis

In this analysis, a microcavity with propagation constant *k* is assumed with an ideal coupler [29]. The coupling coefficient from the coupler to the sphere is taken as *t* and *r* is the part of the field transmitted through the waveguide with the relation $r^2 - t^2 = 1$, since *t* is purely imaginary due to the power conservation. When phase and amplitude contributions are taken into account with the low round trip loss, the quality factor of a spherical microcavity coupler system described in Equation 2.18 can be expressed as

$$Q_{total}^{-1} = Q_{intrinsic}^{-1} + Q_{external}^{-1} \tag{2.27}$$

where now, $Q_{external}^{-1} = 2\pi ak/|t|^2$, is related to the coupling from the spherical microcavity to the coupler [30].

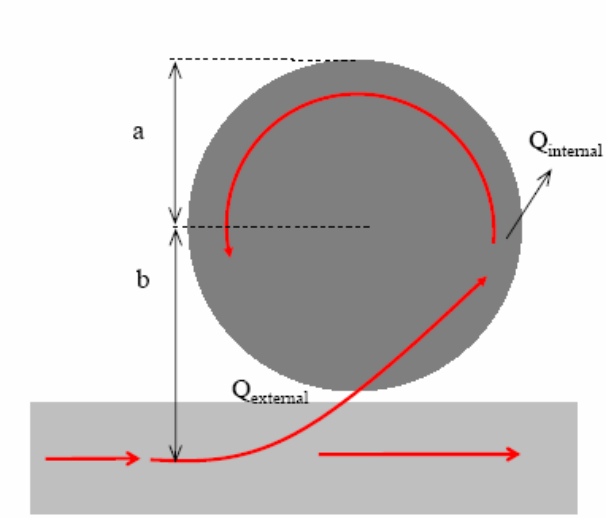

Figure 2.5. Scheme of coupling to the microsphere.

Coupling can be characterized by the fractional depth of the resonance dip in the transmission through the coupler, *K*

$$K = \frac{4Q_{intrinsic}Q_{external}\Gamma^2}{\left(Q_{intrinsic} + Q_{external}\right)^2} \qquad (2.28),$$

where Γ is the mode matching coefficient ($\Gamma \leq 1$). For a single mode coupler, mode matching is always achieved ($\Gamma = 1$). For critical coupling $K = 1$, and hence $Q_{intrinsic}^{-1} = Q_{external}^{-1}$. For nonideal (partial) matching, critical coupling can be achieved with a lower external quality factor, $Q_{intrinsic}^{-1} > Q_{external}^{-1}$ [31]. The external quality factor can be controlled by the microsphere coupler gap. Therefore the critical coupling can be achieved

by the control of the impact parameter, b. In fact, the relation between the impact parameter (b), size parameter (x), and the mode number (n) can be expressed as

$$b = \left(n + \frac{1}{2} \right) \frac{a}{x} \tag{2.29},$$

for MDR excitation. Light coupling to MDR's of a microsphere can still obtained if the condition $N_1 a \geq b \geq a$ is satisfied [32].

2.3.2 Coupling Systems

The standard coupling systems used are demonstrated in Figure 2.6. Tapered fiber is a transcendent coupling apparatus with a gap control. Tapered fibers are fabricated by heating and pulling at the same time to form a narrow waist.

The thickness of the waist can be as small as a micrometer so that the fundamental mode extends out of the fiber [33, 34]. The obvious disadvantage of tapered fiber coupling is the easy deterioration of highly sensitive and fragile narrow waist.

Buried waveguide coupler is made up of a phase-matched waveguide channel. Efficient coupling with this system is rather difficult, however the most robust and compact coupling system is the buried waveguide coupling [35].

Prism coupling is the oldest system used for evanescent wave coupling. Phase matching is crucial in prism coupling. Proper incidence angle and refractive indices for the prism and the microsphere has to be selected. This system is also robust, however the optical alignment is difficult [36].

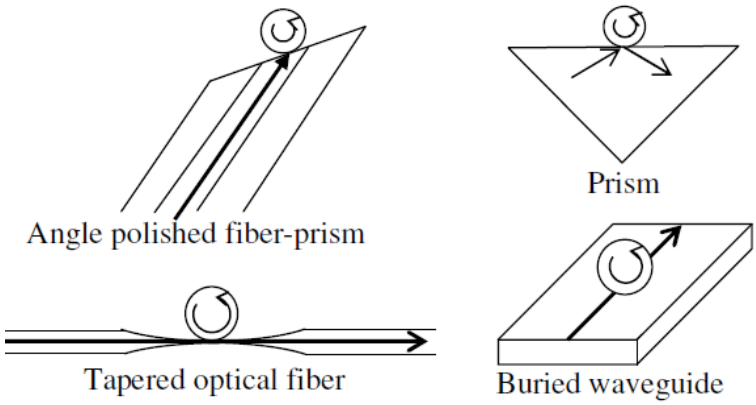

Figure 2.6 Common coupling geometries.

The fiber-prism coupling provides the joint advantages of fiber and prism coupling. In this case, waveguide light insertion is provided with the fiber, and a robust coupling is achieved with the prism [37].

There is also one other coupling technique with the use of an optical fiber half coupler (OFHC). In a similar concept with an integrated waveguide, but with easier fabrication, an OFHC has the advantages of fiber coupling. A single mode fiber is placed into a glass block. Then the whole block is polished with the fiber embedded in the block until an efficient coupling distance is achieved.

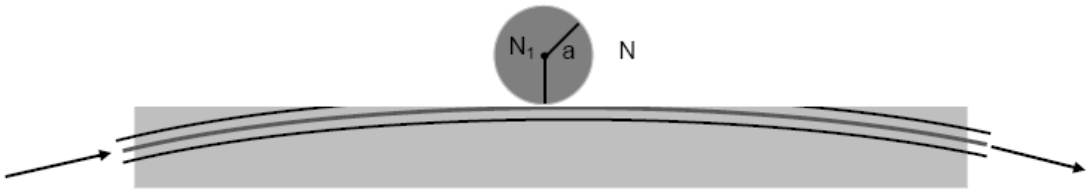

Figure 2.7 Side view of the optical fiber half coupler (OFHC).

In the experiments, single mode OFHC's at 1.5 μm and 1.3 μm are used. The cladding diameter of the fiber is 125 μm and the core diameter is on the order of 10 μm. For

efficient coupling, the microsphere has to be perfectly placed. However, this is rather challenging, when microspheres with diameters smaller than 100 μm are used.

Chapter 3

MDR'S AS TRANSDUCING MECHANISMS

3.1 Introduction

MDR's are very high Q factor optical resonances with properties dependent on the size, shape and the refractive index of the resonator. High Q factors imply very low resonance linewidths, and even very tiny changes in the morphology of a resonator show up as shifts in the resonances. Changes in the morphology of a resonator can be induced in several ways. For example, thermal changes induce change in the refractive index and the size of the resonator. Another example is a particle polarized by the evanescent field of a MDR. In this case, the polarizing particle induces a change in the optical path of the mode in the resonator. Hence, this can be thought as a change in the geometry of the resonator.

3.2 Thermo-optic effect

The dependence of the refractive index on the temperature is essential for designing temperature sensitive tools and analyzing temperature instabilities. Either dielectric or semiconductor, every material has a thermo-optic coefficient used in describing the relation between the refractive index and temperature. Furthermore, temperature changes can also alter the size of the microsphere, which leads to a geometrical change in the resonator. However, thermal expansion is negligible when compared to thermo-optic effect in most materials. The relation between the relative refractive index and the temperature is given as

$$\Delta M = \frac{dM}{dT}\Delta T \qquad (3.1),$$

where ΔM is the change of refractive index of the resonator, dM/dT the thermo-optic coefficient of the resonator material and ΔT the change in temperature. Thermo-optic coefficients of microspheres used in the experiments of this work are 1.2×10^{-5} K^{-1} (silica) and 2×10^{-4} K^{-1} (silicon) [38]. Note the order of magnitude difference between the silica and the silicon. The change in the resonance wavelength can be found from

$$\lambda(\Delta T) = \lambda(0)\left(1 + \frac{\frac{dM}{dT}\Delta T}{M_{eff}}\right) \tag{3.2},$$

where $\lambda(\Delta T)$ is the resonance wavelength after temperature change, $\lambda(0)$ is the resonance wavelength before temperature change [39]. Also, it is important to emphasize that the temperature change can be due to conventional heating of the cavity [40], from surface chemical effects [41], from carrier injection by electric voltage [42] and from absorption and thermal relaxation of the electromagnetic field which excites the morphology dependent resonance.

3.3 Change of optical path by particle adsorption

A particle that is adsorbed on the surface of a microsphere can be detected by a shift in the MDR's because of the perturbation caused by the particle. Consider a microsphere coupler system at a resonant wavelength. The binding of a particle increases the optical path of the photon orbit and the microsphere is no more resonant at that wavelength. The perturbation can be analytically described by characterizing the particle with its excess polarizability (α_{ex}), and the shift in the resonant wavelength is expressed as

$$\frac{\delta\lambda}{\lambda} \approx \frac{\alpha_{ex}\sigma_s}{\varepsilon_0\left(N_1^2 - N^2\right)a} \tag{3.3},$$

where, σ_s the surface density of the particles, ε_0 the vacuum permittivity and N_1 and N the refractive index of the resonator and the solution, respectively [43]. Even though MDR's of microspheres are characterized in air, particle or molecule detections are done in solutions [44]. Hence, the experiments are performed in solutions and the analytical expressions include the refractive index of the solution.

3.4 Electro-optic effects

Electrically induced optical effects steer applications in optical signal processing by making use of materials that are electro-optically active. There are several mechanisms responsible for optical changes (the refractive index and/or in absorption of the material) by applying an electric field. Devices such as electro-optic modulators are widely used and are based on the phenomena like Kerr effect, Pockels effect, carrier injection (or depletion), and Franz-Keldysh effect. When the resonator material is electro-optically active, MDR's can also be shifted, and hence tuned. Shift of MDR's by electro-optic effects and electro-optic modulation have been observed in microspheres made of silicon and crystalline quartz [45, 46]. Hence, it is essential to explain the mechanisms that cause electro-optic effects.

Kerr effect is a second order nonlinear effect that materials exhibit under electric field by a change in the refractive index [47]. Kerr effect is dominant in certain liquids, although all materials show it. The relation between the electric field and the refractive index change ΔN is given by

$$\Delta N = \lambda K E^2 \qquad (3.4),$$

where K is the Kerr coefficient, λ the wavelength of the light and E the applied electric field [42].

Pockels effect is different from the Kerr effect with the dependence of the refractive index (first order) on the applied electric field. Materials (crystals) that do not have inversion symmetry show Pockels effect. In Pockels effect, applied electric field induces a birefringence, that is proportional to the magnitude of the field. Lithium niobate is one of the most common crystals used in electro-optical modulators, which use Pockels effect [48].

Franz-Keldysh effect is defined as the distortion of energy bands with the application of electric field, which is predominant at wavelengths that correspond to the band gap of the semiconductor, and exhibits changes in both the optical absorption and the refractive index of a semiconductor under the applied electric field [40, 48].

Carrier injection (or depletion) is another electro-optical effect, which is observed in semiconductors. Change of free carriers results in a change in the absorption and the refractive index of a semiconductor. Recently, electro-optical modulation with MDR's of silicon microspheres has been studied [49].

3.5 Electro-optic effect in Nematic Liquid Crystals

Liquid crystals are liquids with an ordered arrangement of molecules. Liquid crystals posses both crystalline solid and liquid properties. Anisotropy of the mechanical, optical, electrical and magnetic properties of liquid crystals results from the molecular anisotropy. Molecular anisotropy is apparent in two ways; liquid crystal molecules are either rod-like or disc-like in shape. Rod-like shaped liquid crystals give rise to smectic and nematic phases. In nematic phase, liquid crystals are aligned almost parallel to each other along their long axis. Nematic phase shows orientational order, which is the preferred orientation in the neighborhood of any point in the liquid crystal medium at any time at any point. The direction of this preferred orientation is denoted by $\hat{n}$ and is called the director. The director is constant in a homogeneous medium, however in an inhomogeneous nematic liquid crystal (NLC) medium the director can change from point to point. Hence the orientational order parameter of a NLC is defined as

$$S \equiv \left\langle \frac{3}{2}\cos^2\theta - \frac{1}{2} \right\rangle \tag{3.5},$$

where brackets denote a statistical average and θ is the angle between the long axis of a molecule and the director.

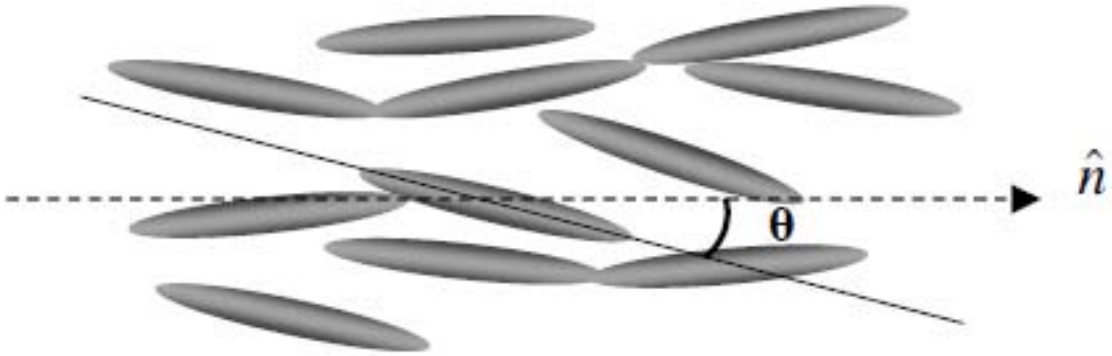

Figure 3.1 Orientational order in a nematic liquid crystal.

Order parameter, $S = 1$, for a perfect parallel alignment and $S = 0$, for a totally random orientation. Due to the orientational ordering, NLC's have uniaxial symmetry with the axis of symmetry being the axis of director. Uniaxial symmetry, results as a dielectric anisotropy between the director axis ($\underline{\underline{\varepsilon}}$) and the axis perpendicular to the director ($\varepsilon_\perp$), which is defined as

$$\Delta\varepsilon \equiv \varepsilon_\perp - \underline{\underline{\varepsilon}} \tag{3.6}.$$

Note that the mean dielectric constant is defined as

$$\bar{\varepsilon} \equiv \frac{2\varepsilon_{\perp} + \underline{\underline{\varepsilon}}}{3} \tag{3.7}.$$

Dielectric anisotropy is the most important property of NLC's for their electro-optical applications. In order to illustrate this, let us consider an externally applied electric field, which induces a dipole moment on the molecules because of their dielectric anisotropy. When the orientational order is not parallel to the applied electric field, a net torque will be exerted on the liquid crystal molecules.

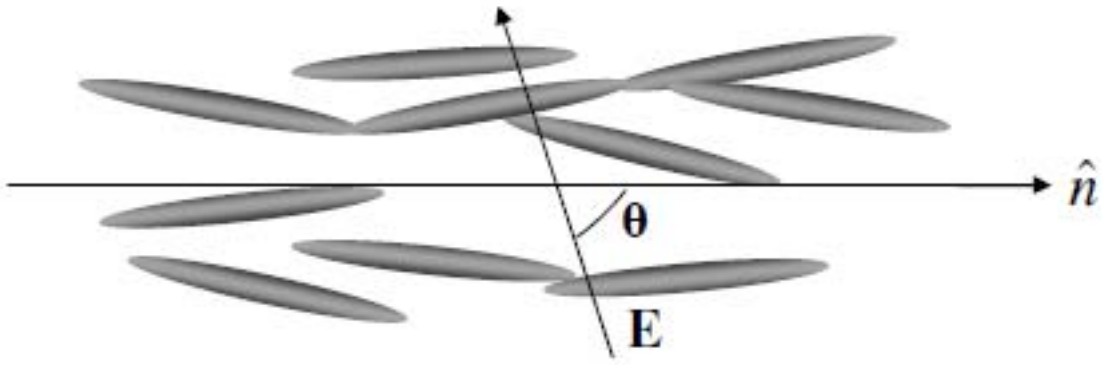

Figure 3.2 Applied electric field and the nematic liquid crystal.

The electrostatic energy then can be written as

$$U = \iiint \left\{ \frac{1}{2}\varepsilon_0 \varepsilon_{\perp} \left|\vec{E}\right|^2 + \frac{1}{2}\varepsilon_0 \Delta\varepsilon \left(\vec{E} \cdot \vec{\vec{n}}\right)^2 \right\} dv \tag{3.8},$$

where $\vec{E}$ is the electric field, and θ is the angle between the electric field and the orientational order [50].

NLC's seem as an opaque and milky liquid in a glass container. This is because of the scattering of light from the boundaries of domains, which have random orientational orders

with respect to each other. The reason for scattering at the boundaries is the refractive index discontinuity. With a proper alignment of the liquid crystal, uniaxial optical symmetry can be observed. The birefringence of the NLC can be expressed as

$$\Delta N = N_e - N_o \tag{3.9},$$

where N_e is the extraordinary refractive index and N_o is the ordinary refractive index. Liquid crystals exhibit two types of birefringence.

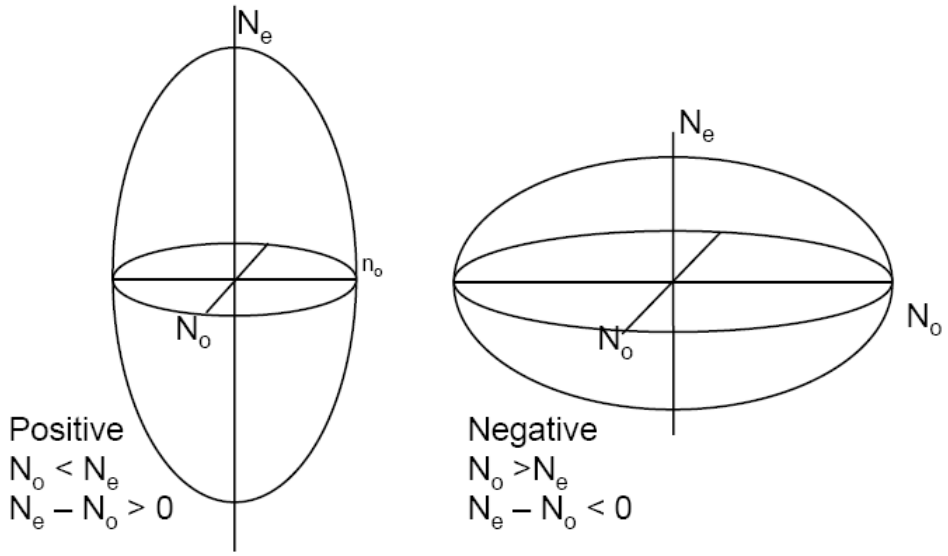

Figure 3.3 Illustration of (a) negative, and (b) positive, birefringence in NLC's.

When $N_e > N_o$, the liquid crystal is called as positively birefringent and when $N_o > N_e$, the liquid crystal is called negatively birefringent. The refractive index that a photon experiences at any angle can be calculated with the following equation,

$$N(\theta_p) = \frac{N_e}{\sqrt{\cos^2\theta_p + \frac{N_e^2}{N_o^2}\sin^2\theta_p}} \quad (3.10),$$

where θ is the angle between the polarization of the incoming photon and the extraordinary axis of the NLC. Liquid crystals show elasticity like many solids and liquids.

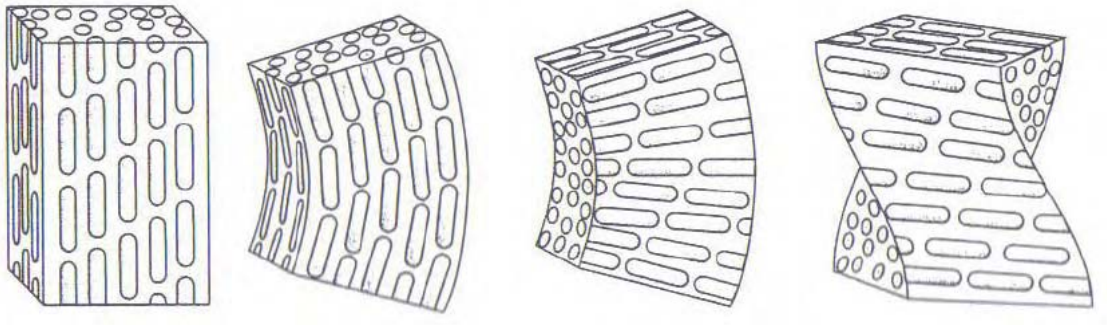

Figure 3.4 Illustration of (a) bend, (b) splay, and (c) twist deformations [51].

When a liquid crystal system is perturbed from an equilibrium conformation, the elastic constants determine the restoring torques. In applications, usually the balance between the electric torque and the elastic restoring torque determines the liquid crystal pattern. Any deformation of liquid crystals is the combination of the three basic deformations; bend, splay and twist deformation, which are expressed respectively in the terms of the following equation [52, 53, 54].

$$F_{elastic} = \iiint\left(\frac{1}{2}k_1\left|\vec{\nabla}.\hat{n}\right|^2 + \frac{1}{2}k_2\left|\hat{n}.\vec{\nabla}\times\hat{n}\right|^2 + \frac{1}{2}k_3\left|\hat{n}\times\vec{\nabla}\times\hat{n}\right|^2\right)dv \quad (3.11).$$

The orientation of the NLC is due to the minimization of free energy (F), which is written in terms of elastic and electrostatic energy

$$F = F_{elastic} - U \quad (3.12),$$

where U is as expressed in equation 3.8.

The nematic liquid crystal (NLC) used in the experimental part of this work is 4-pentyl-4'-cyanobiphenyl (5CB). The molecular structure is given in Figure 3.4, the refractive indices at 1.4 μm wavelength are N_o = 1.51 and N_e = 1.67 [55]. Elasticity coefficients are $k_1 = 6.4$, $k_2 = 3$, $k_3 = 10$. 5CB is in nematic phase between the temperatures, 24˚C-35˚C [56].

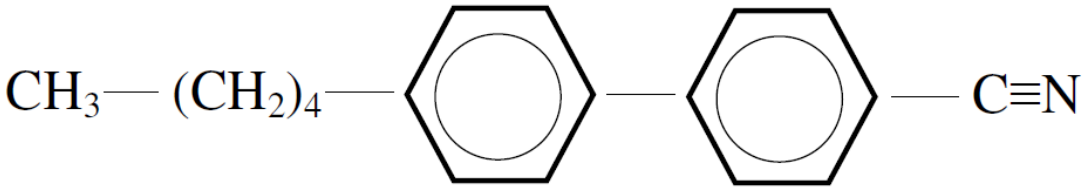

Figure 3.5 Chemical structure of 4'-pentyl-4-cyanobiphenyl or 5CB.

Combining the optical properties of liquid crystals with the high Q factors of spherical microcavities is a relatively new idea. Morphology dependent resonance tuning has been demonstrated with liquid crystal droplets [57]. Dye doped nematic liquid crystals droplets of sizes 10 μm to 30 μm, embedded in a polymer matrix have exhibited electrical tunability. Tunability is achieved by inducing a change in the refractive index pattern of the spherical microdroplet with applied electric field. The idea of use of solid microspheres with liquid crystals adds robustness to the liquid crystal-optical cavity system. Using nematic liquid crystals (NLC's) as the outer medium for microspheres gives rise to the tunable effective refractive index of the microspheres [50].

Chapter 4

ELASTIC LIGHT SCATTERING AND MODULATION

4.1 Experimental Setup

In the experimental part of this work, silicon and silica microspheres are used. MDR's are excited with various distributed feedback (DFB) diode lasers, that are controlled by the laser diode controller (LDC) through a computer via a user interface (National Instruments Labview®) program.

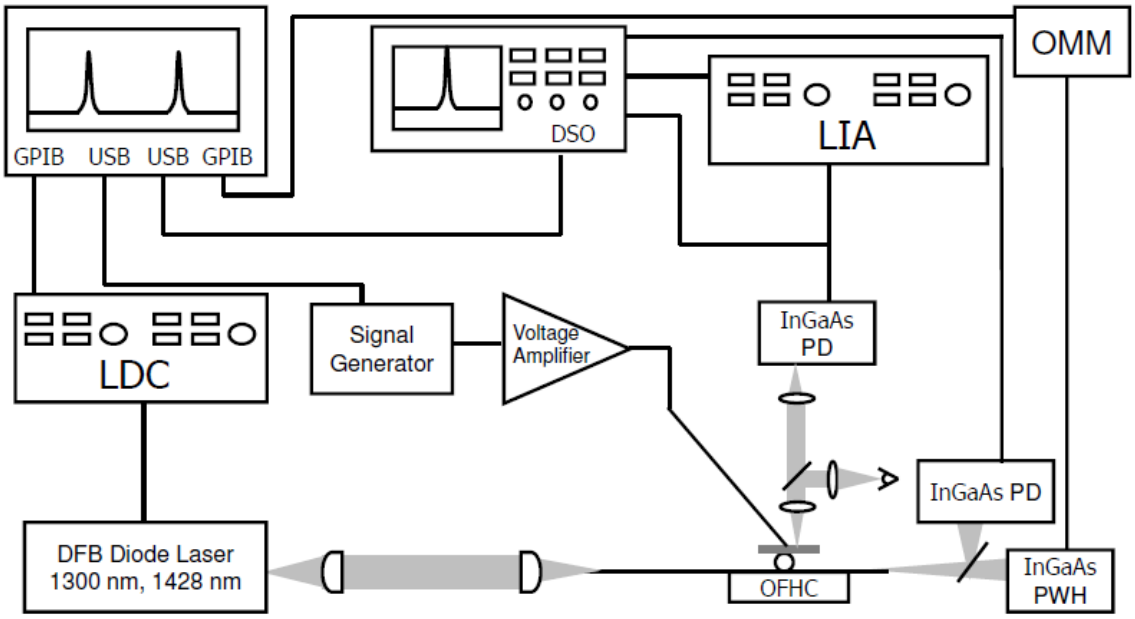

Figure 4.1 The schematic of the experimental setup.

The program controls the temperature hence the wavelength of the diode laser with a combination of a Peltier cooler and a thermistor within the user-defined parameters, such

as the current to the Peltier cooler. The current steps determine the wavelength scanning steps. The temperature-wavelength curve of the diode laser sets the resolution in scanning the wavelength. The temperature wavelength curve is obtained by the help of the optical multimeter (OMM). The wavelength of the laser light is measured by the OMM and with a third order polynomial fit, calibration of the exact wavelength is obtained. In figure 4.2, the measured wavelength and the calibration curve is plotted as a function of temperature.

The microspheres used in the experiments have sizes of a hundred microns to millimeters, hence the mode spacing of the resonances is relatively small (recall Equation 2.27 and 2.30). Therefore the calibration is crucial for the detection of narrow linewidth, low mode spacing resonances.

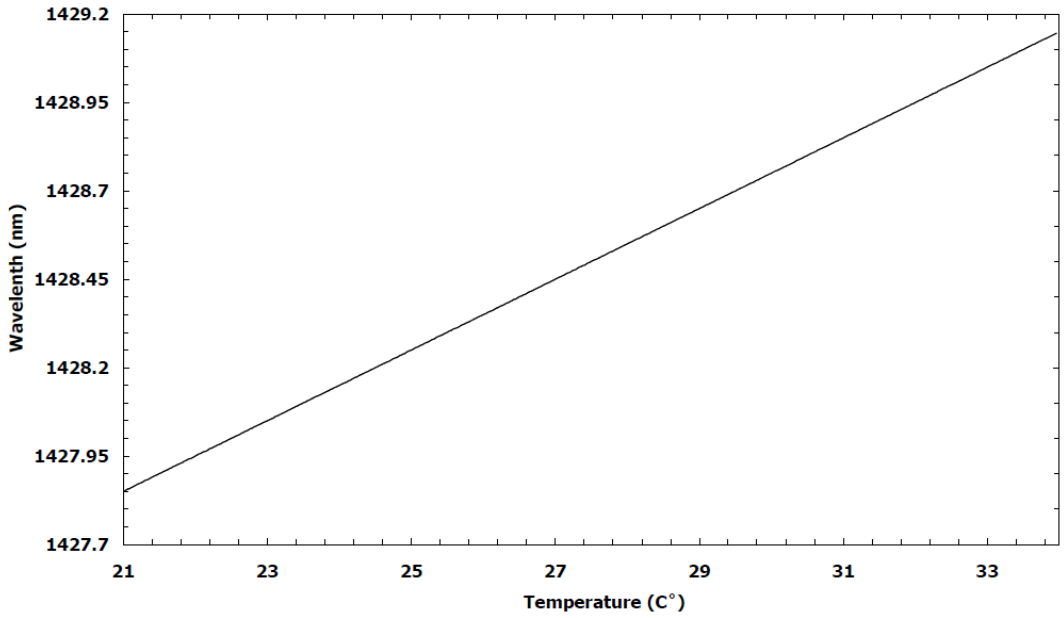

Figure 4.2 The calibrated laser diode wavelength versus temperature.

The two lasers used in the experiments are a 1300 nm DFB free space laser and a 1430 nm fiber pigtailed DFB diode laser. Also various OFHC's have been used to couple various wavelength light sources to the microspheres. In order to couple the free space

laser into the single mode OFHC at 1300 nm with core diameter of 10 μm and refractive index of 1.44, two aspheric lenses are used with focal lengths 4.5 mm and 3.1 mm. The lenses and the fiber are controlled with XYZ stages and the coupling is limited by the mechanical resolution of the stages, which is 1 μm. Silica microspheres are around 100 μm in size and are controlled with two microelectronic probes, whereas silicon microspheres (1 mm in size) are controlled by another XYZ stage with a microscope glass on top of the sphere. The microscope glass touching the silicon sphere from the top provides both the precise control of the microsphere on the OFHC and provides an upper surface for the use of liquids and liquid crystals as the outer medium.

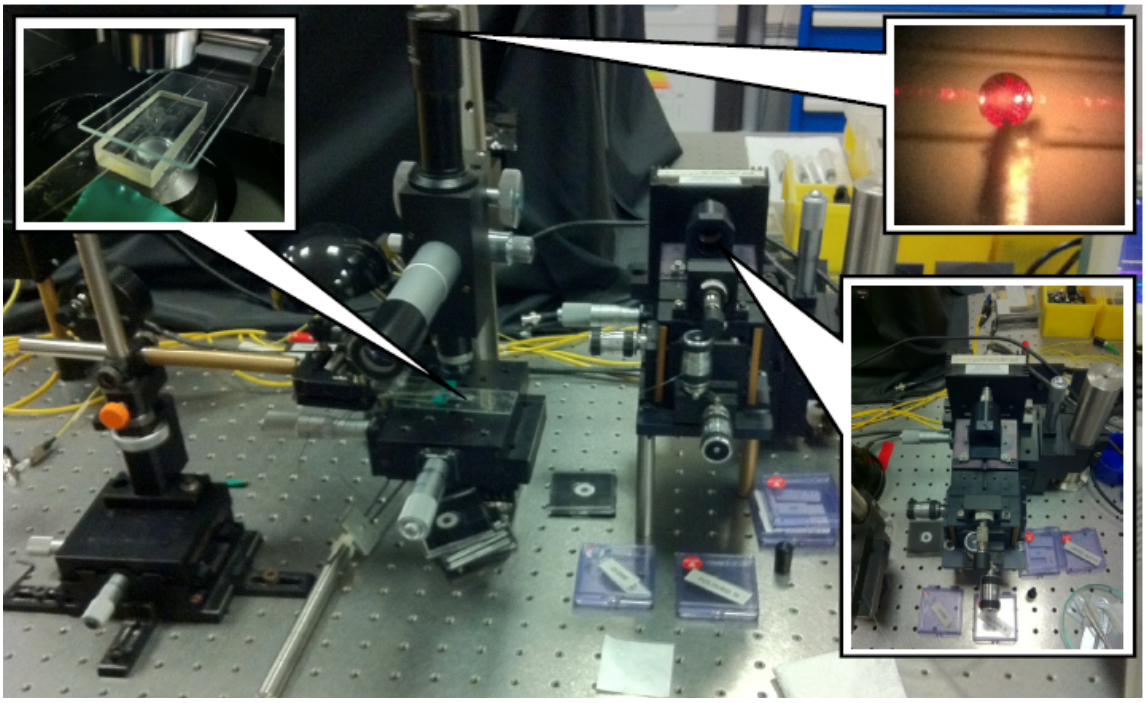

Figure 4.3 The photograph of the experimental setup.

Aluminum electrodes are placed on the below surface of the glass slide for switching the liquid crystal in the silicon microsphere-nematic liquid crystal MDR tuning and modulation experiments. The elastically scattered light from the microsphere at 90˚ is

collected by an InGaAs photodiode (PD) and with the help of a microscope, which has a total magnification of 50X or 100X (with a 5X or a 10X objective lens and a 10X eyepiece). The light transmitted through the fiber is collected by another InGaAs photodiode (PD) or the InGaAs power wave head (PWH) connected to the OMM. Using the PWH is helpful in reducing the electronic noise in the PDs, since the data is acquired and processed internally. However, the response of the OMM is quite slow for modulation experiments. For modulation experiments, 90˚ elastic scattering intensity is amplified with a lock-in amplifier (LIA). The transmitted, scattering and the amplified signals are monitored on the digital storage oscilloscope (DSO) and recorded in the computer via the National Instruments Labview® software.

4.2 MDR's of Dielectric Microspheres in Air and in 5CB

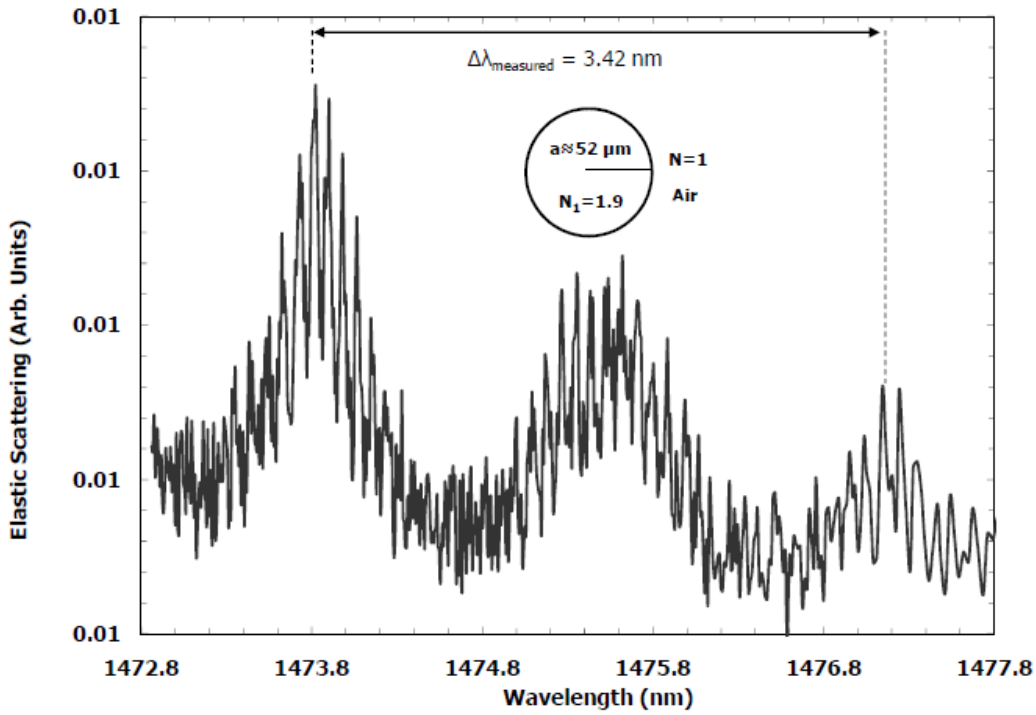

Figure 4.5 Elastic scattering spectra of silica microspheres in air.

Dielectric microspheres used in these experiments are high refractive index ($N_1 = 1.9$), Titanium oxide doped silica microspheres. High refractive index allows the silica microspheres to be used in the liquid crystal medium. However excess amount of liquid crystal on the OFHC results in non-resonant coupling and scattering of light through the liquid crystal molecules. Figure 4.5 shows unpolarized elastic scattering spectra from a high refractive index silica microsphere of specified size of 103 μm. By the help of the equation 2.30, the size of the microsphere can be estimated as 125 μm. The difference between the specified and the measured value is due to the variations in the specified sizes. The silica microspheres are controlled on the OFHC by the use of Tungsten probe tips that are as thin as 20 μm.

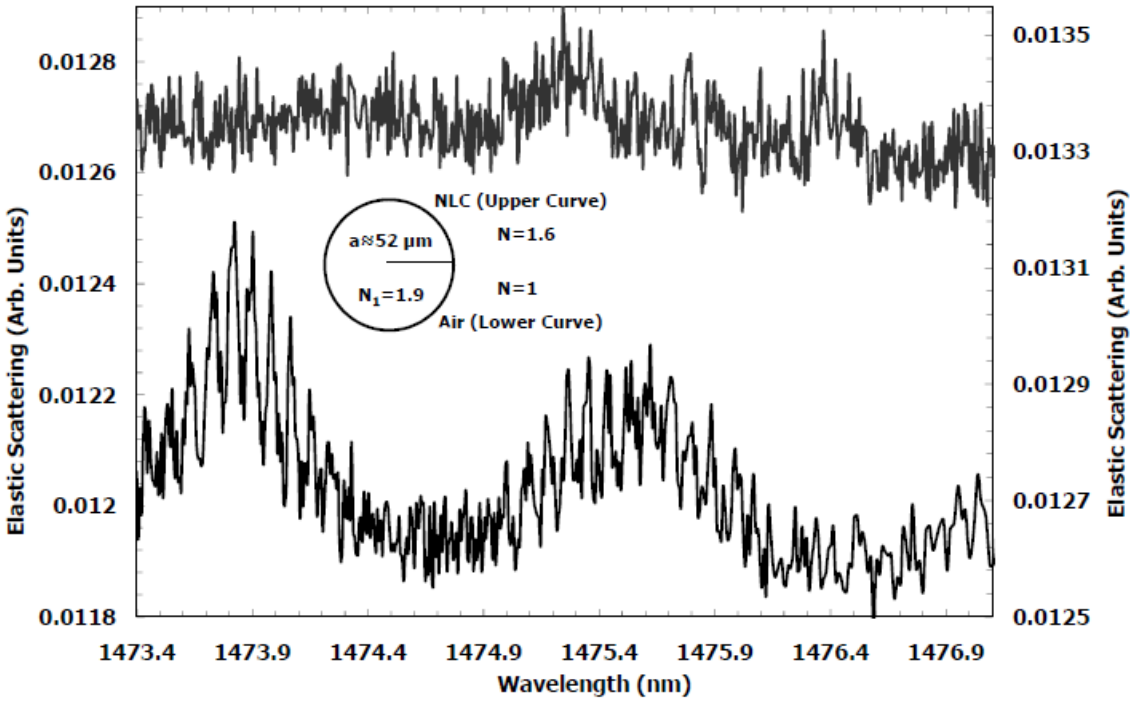

Figure 4.6 Elastic scattering spectra of silica microspheres in air and NLC (5CB).

The upper curve in Figure 4.6 is the elastic scattering from a Ti oxide doped silica microsphere in NLC, where the below spectrum is obtained in air.

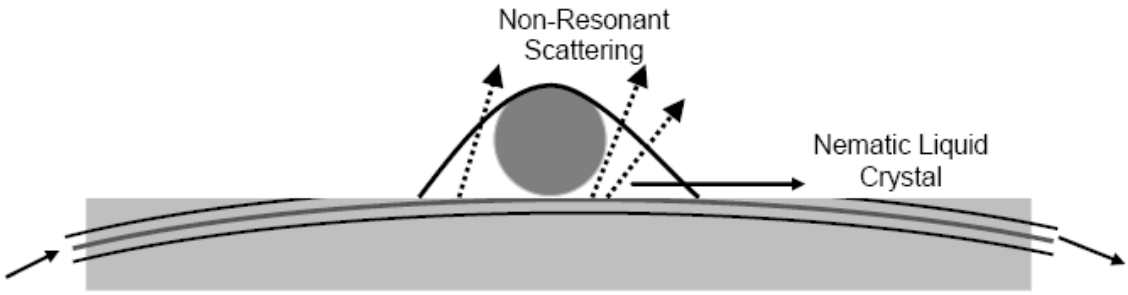

Figure 4.7 Illustration of non-resonant scattering because of NLC (5CB).

The morphology dependent resonances are no longer observable when the liquid crystal coats the microsphere, because of the high refractive index of 5CB (1.51-1.67) when compared to that of the silica OFHC (1.44).

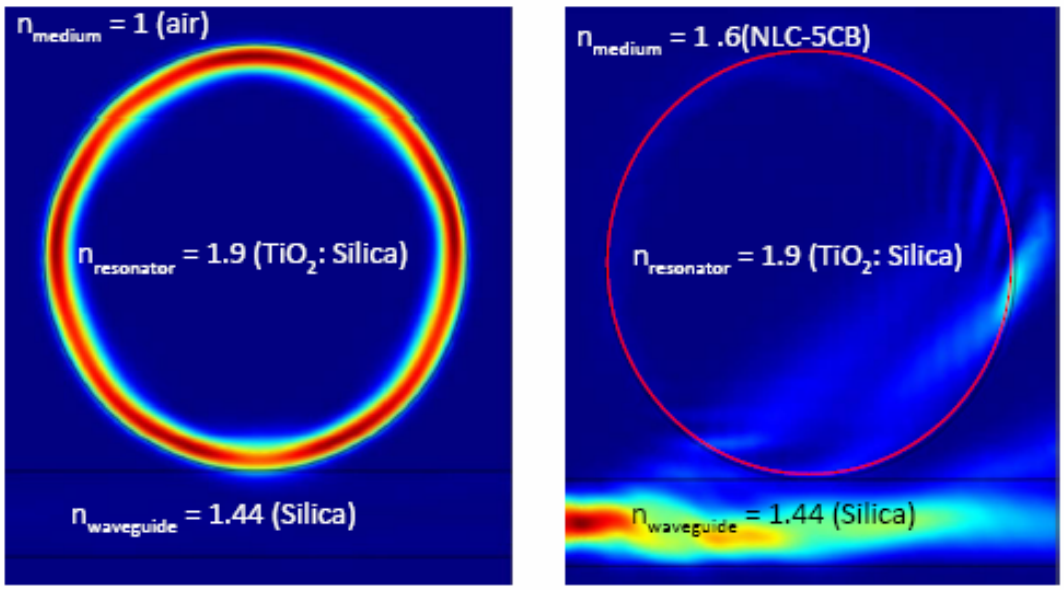

Figure 4.8 TE EM wave intensity for a resonator in (a) air and (b) 5CB.

The effect of non-resonant scattering is simulated in a two dimensional, cylindrical microcavity for which the MDR's are excited with a waveguide of refractive index 1.44 in two media with refractive indices lower and higher than that of the waveguide. In order to remove the scattering of input light by the liquid crystal molecules, the interaction of microspheres with NLC's can be restricted only to the top portion of the microsphere. For this purpose, a scheme with small 5CB drops generated on a glass piece with ITO electrodes is designed. Silica microspheres are intended to be suspended in 5CB drops by the surface tension of the NLC. However the difficulty in the alignment of such small microspheres on OFHC requires the use of bigger microspheres.

4.3 MDR's of Silicon Microspheres in Air

Silicon microspheres with sizes of 1 mm are investigated for their MDR's in air at first.

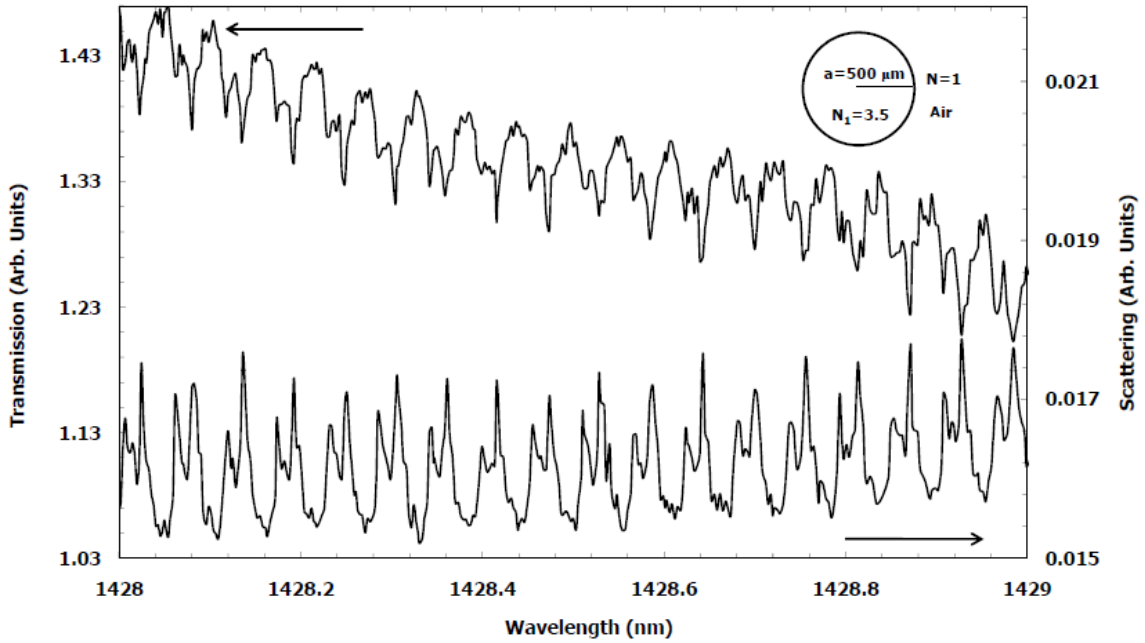

Figure 4.9 Elastic scattering and transmission spectra of silicon microspheres in air.

Due to the high refractive index (3.5) and the large size of the silicon microspheres, MDR's are very narrow in linewidth and dense in the elastic scattering spectra. With unpolarized input light, both TE and TM modes are excited and a complicated spectrum is expected.

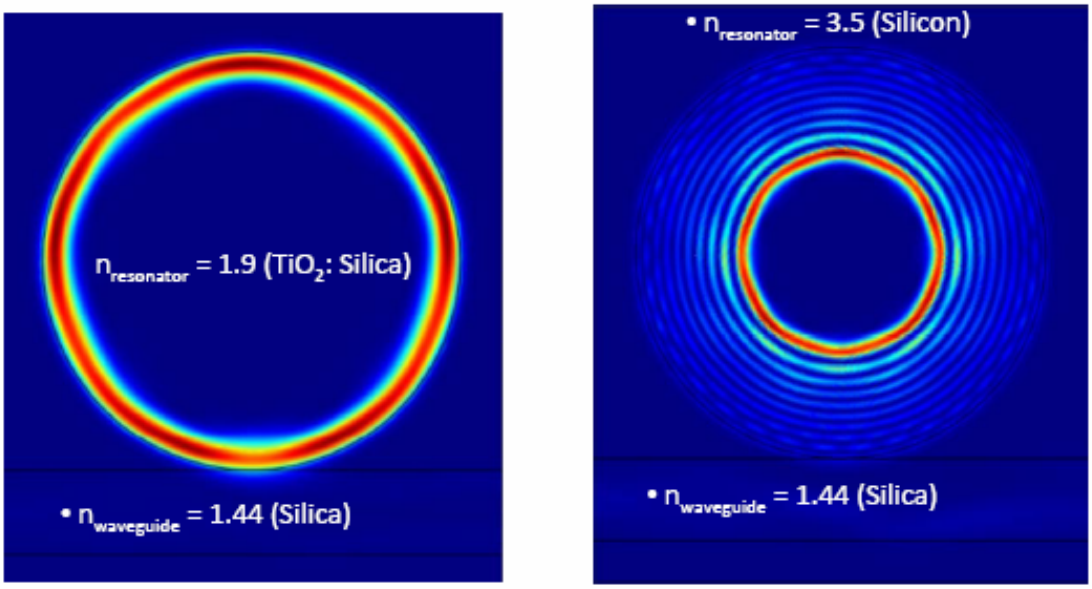

Figure 4.10 TE EM wave intensity for (a) silica and (b) silicon resonator.

Observation of resonances with different mode numbers is instrument limited because of the excessive number of radial and polar modes with both TE and TM polarizations. Hence, the measured resonances are actually a collection of resonances with different radial mode numbers and the number of resonances in one mode spacing is related to the resolution of the measurement. The calculated mode spacing is 0.248 nm and finding peaks or dips with such spacing is possible in the obtained spectra. MDR's are observed as peaks in the 90˚ elastic scattering and dips in the transmission through the OFHC.

Figure 4.9 shows the transmitted and the elastically scattered spectra for a silicon sphere in air. When the light is at resonance in the cavity, light is confined and the power is

not transmitted through the OFHC but contained in the cavity. Note the difference in the mode spacings of silica and silicon microspheres in air. In the spectra, the wavelength is scanned for 1 nm for observation of tens of MDR's in a silicon microsphere, whereas the wavelength was scanned for 3.5 nm for silica microspheres in order to observe a few MDR's. This is of course due to the large difference in the size and the refractive index of the two microspheres.

The radial propagation of optical intensity in high refractive index cylindrical microcavities is simulated and shown in Figure 4.10. The caustic zone of the resonator with high refractive index (silicon) is much less than the caustic zone of the resonator with low refractive index (silica). Hence the number of radial modes is significantly higher in high refractive index, e.g. silicon, microresonators.

4.4 MDR's of Silicon Microspheres in Water

Observation of MDR's in aqueous solutions is important for biochemical sensing applications, since sensing experiments are mostly performed in solutions. Since the refractive index of the water is 1.32 at 1430 nm, the background of the scattering signal increased and the background of the transmission signal decreased with respect to those in air. Ideally, water is a homogeneous medium. However in the experiment, the contaminants have to be taken into consideration and the relatively low Q factors of MDR's in water can be attributed to the losses due to the scattering of the particles staying on the surface of the silicon microsphere. The mode spacing of MDR's of silicon microspheres are slightly different in air and in water. The mode spacing has decreased due to the effective refractive index change of the silicon microsphere.

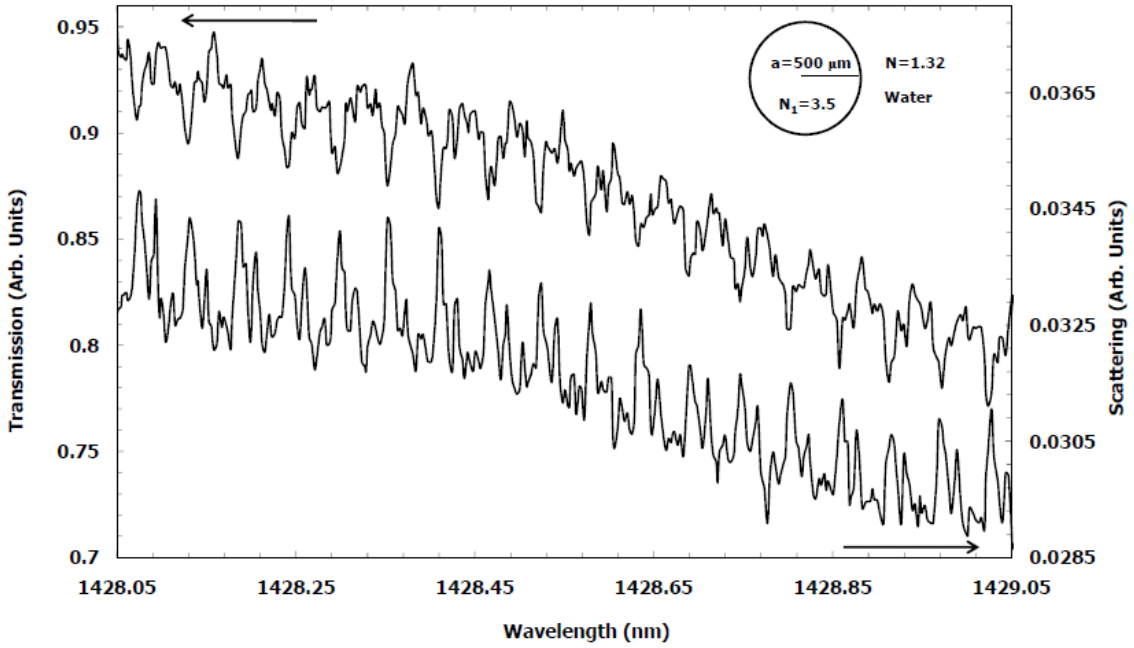

Figure 4.11 Elastic scattering and transmission of a Si μ-sphere in water.

Calculated mode spacing is now 0.237 nm. This is confirmed by the measurement. The number of peaks and dips in figure 4.11 has increased as predicted by the theory.

4.5 MDR's of Silicon Microspheres in Ethylene Glycol

Ethylene glycol (EG) is a pure, colorless organic molecule with a refractive index of 1.41, which is lower than that of the fused silica. Even though the background signal increases in scattering and decreases in transmission, the pure and homogeneous structure of the molecule leads to high Q factor measurements of MDR's of silicon microspheres in EG. The Q factors in ethylene glycol medium are even comparable or better than the Q factors measured in air. The reason for this fact may be the removal of present contaminants from the surface of the silicon microsphere with excessive addition of ethylene glycol.

The highest Q factors measured are around 10^6, which is instrument limited. The predicted mode spacing for 1 mm silicon microspheres in ethylene glycol is 0.234 nm. Again finding peaks and dips with predicted mode spacing distance is possible and the mode spacing change is observable in Figure 4.12.

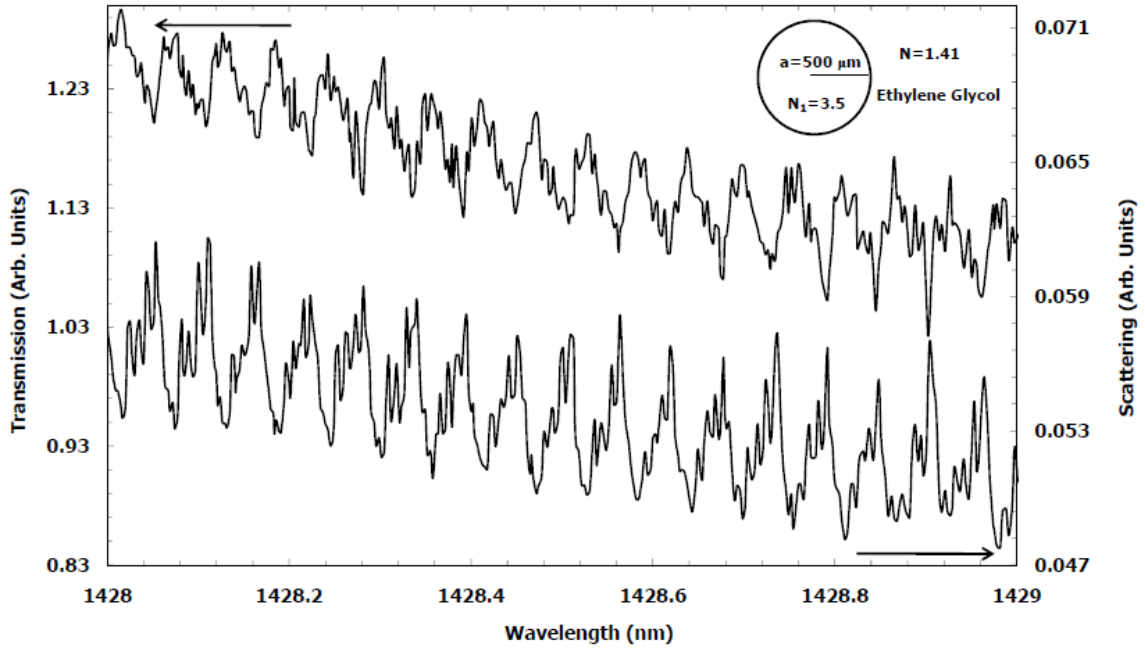

Figure 4.12 Elastic scattering and transmission of a Si μ-sphere in EG.

4.6 MDR's of Silicon Microspheres in NLC's

So far, the effect of change of effective refractive index on the MDR's of silicon microspheres by surrounding medium change has been investigated. Nematic liquid crystals (5CB) provide the possibility to change the morphology of the microsphere within itself. A glass slide with aluminum electrodes on its surface is used to precisely control the place of the silicon microsphere on the OFHC. Moreover, the gap between the aluminum electrodes is filled with 5CB to interact with the silicon microsphere only from the top of the sphere. The highly scattering orientational structure of 5CB easily degrades the MDR's

of a silicon microsphere. Even very small amounts 5CB can result in a very large amount of scattering. In the experiments with the 5CB medium, PWH and OMM are used to collect the transmission through the OFHC.

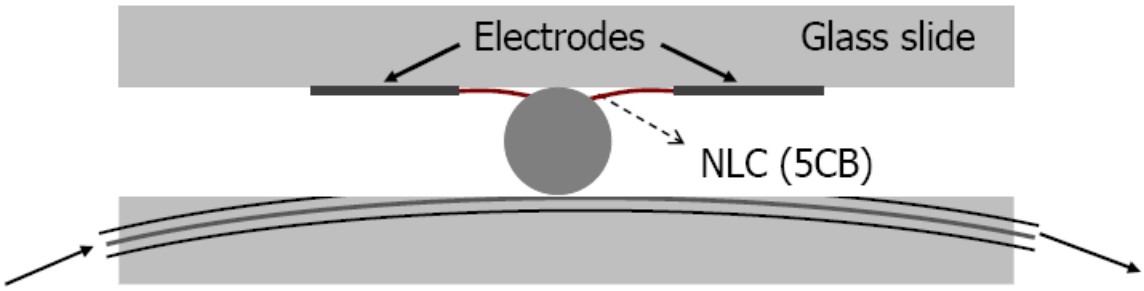

Figure 4.13 Illustration of Si μ-spheres with the top NLC (5CB) contact.

Figure 4.14 shows the transmission spectra obtained through the OFHC after interacting with the silicon microsphere-nematic liquid crystal system. The dips in the spectrum correspond to the resonances in the silicon microsphere. The excess number of modes in silicon microspheres of size 1 mm is again exhibited in the transmission spectrum. There are 6 mode families lying along in one mode spacing. Note that, very little amount of 5CB is interacting with the microsphere. The more 5CB interacts with the silicon microsphere, the lower the Q factor of the resonances. This effect is very well demonstrated in figures 4.15 and 4.16.

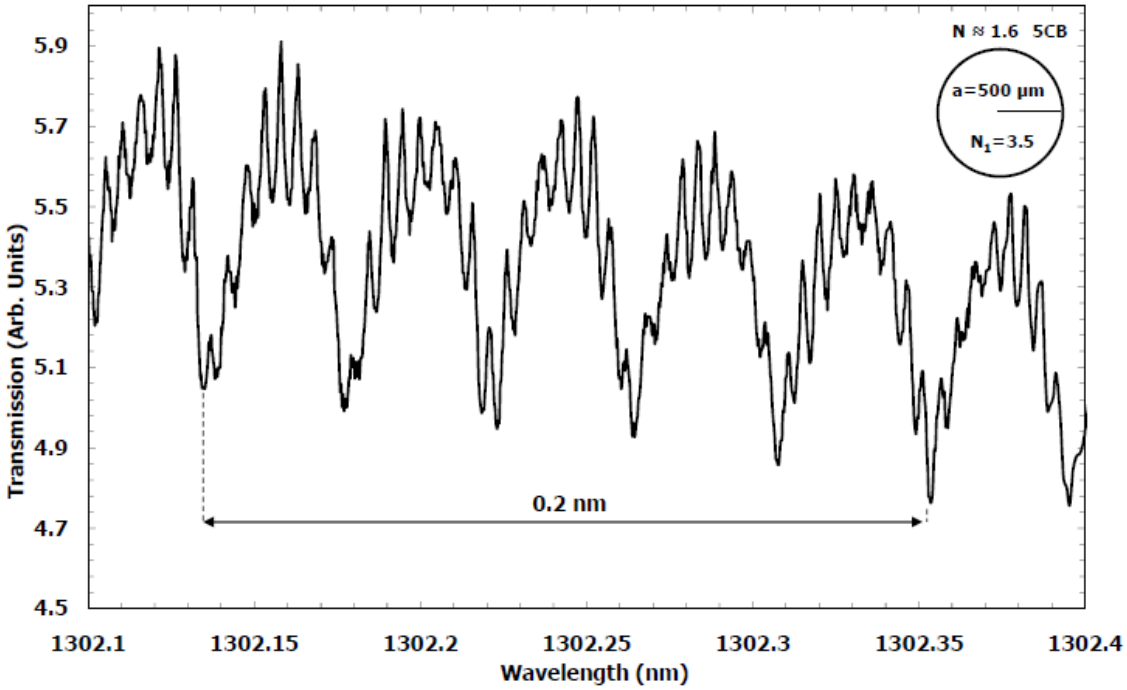

Figure 4.14 Transmission spectra of silicon microspheres in 5CB.

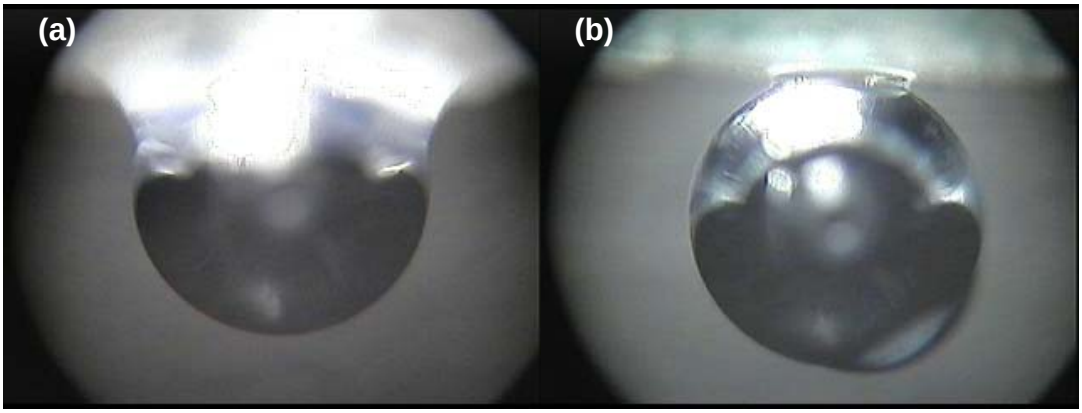

Figure 4.15 Si μ-spheres with (a) excess and (b) little 5CB.

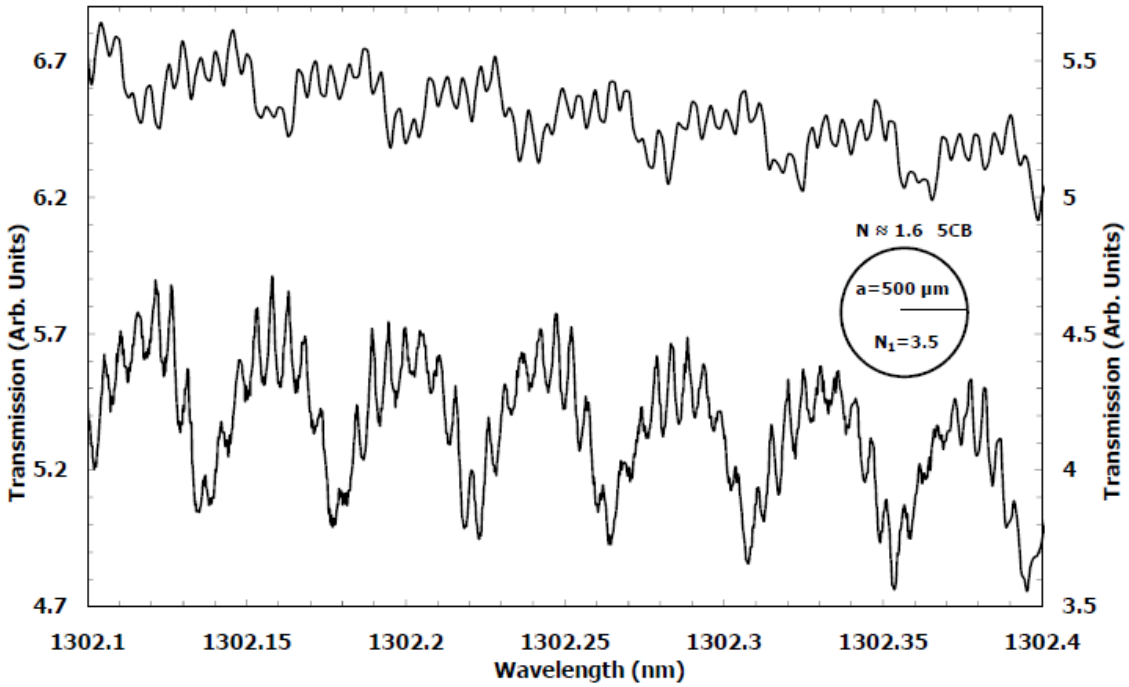

Figure 4.16 Transmission of Si μ-sphere in excess (upper) and little (lower) 5CB.

Two micrographs of silicon microspheres suspended with the surface tension from two different 5CB drops correlate well with the two spectra in Figure 4.16.

Figure 4.17 shows the transmission spectra of the silicon microsphere in NLC. In the upper curve, a continuous waveform (CW) alternating current (AC) electric field (E) with a root-mean-square (RMS) value of 0.4 V/μm is applied to NLC. In the lower curve, no external electric field is applied to the NLC. When the CW external AC electric field is applied to the microsphere, the transmission spectrum shows a red shift of 0.014 nm, corresponding to a change of 10^{-3} %.

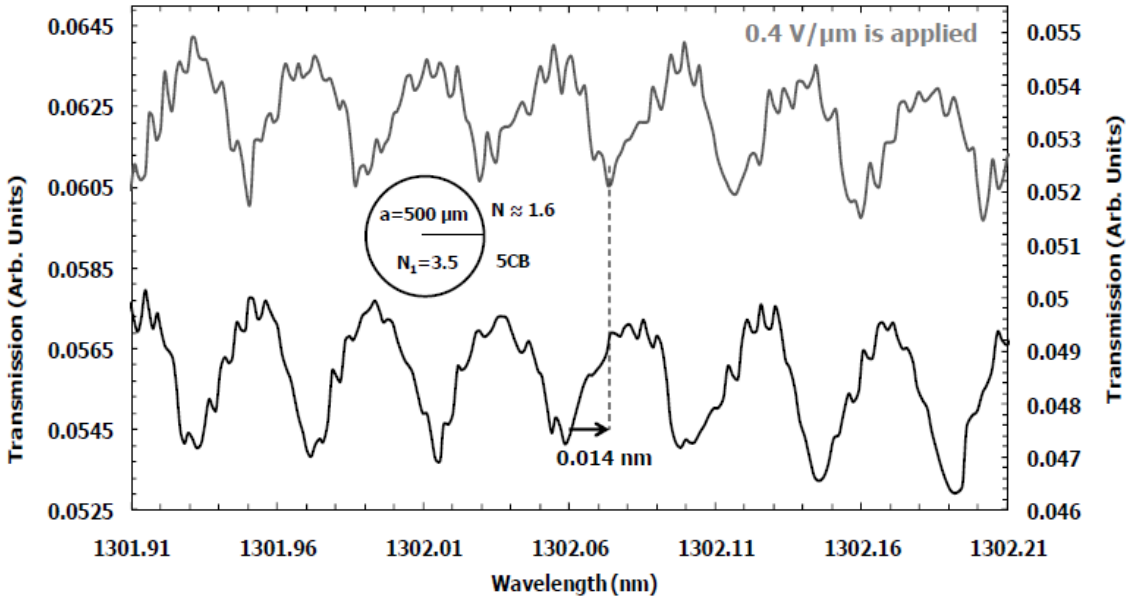

Figure 4.17 Si μ-sphere in 5CB transmission with (upper) & without (lower) AC.

When there is no applied external AC electric field, the NLC molecules are in their rest state. As the external AC electric field is applied, the NLC molecules are expected to orient along the direction of the external AC electric field. The silicon microsphere might also heat up due to an induced AC current. These effects result in the alteration of the relative refractive index of the silicon microsphere and the shift of the elastic scattering and the transmission spectra. This spectral shift gives the opportunity to modulate the amplitude of the elastically scattered and the transmitted light signals from the silicon microsphere, when operating at a constant laser wavelength.

4.7 Modulation with MDR's of Silicon Microspheres in NLC's

In this part of the experiment the shift of MDR's of silicon microspheres with the use of NLC (5CB) as a surrounding medium is studied.

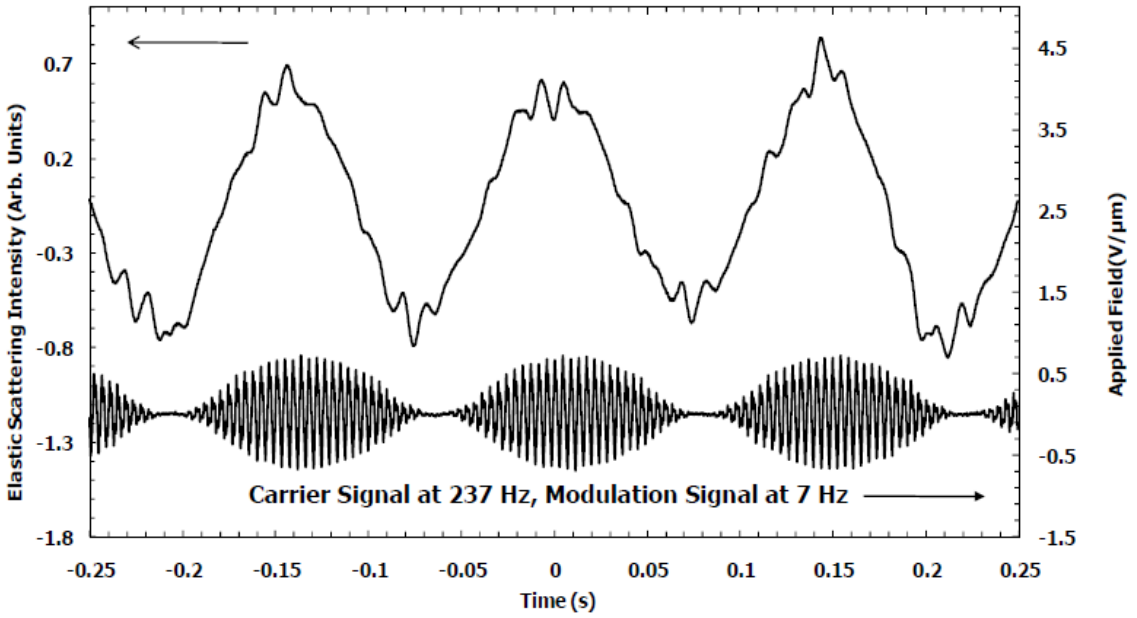

Figure 4.18 The scattering intensity (upper) and the modulating AC field (lower).

Applying a modulated external AC electric field is expected to result in the modulation of the relative refractive index and a modulation of the 90º elastic scattering and the transmitted light intensities from the silicon microsphere. To test this hypothesis, a modulated AC electrical signal is applied to the NLC, as shown in the lower curve of Figure 4.18. The modulation signal of the AC electric field is at 7 Hz, whereas the carrier signal is at 234 Hz. The upper curve of Figure 4.17 shows the 90º elastic scattering intensity, exhibiting a modulation which is in phase with the modulating external AC field.

The tuning and the modulation of silicon microsphere MDR's with a NLC heralds novel optoelectronic applications for liquid crystal on silicon (LCOS) technologies.

Chapter 5

CONCLUSIONS AND FUTURE WORK

This work studies the morphology dependent resonances (MDR's) of dielectric and semiconductor microspheres for their potential applications in liquid crystal technologies. Optical resonances of microspheres in organic and crystalline liquids and aqueous media have investigated.

In the second chapter, "light scattering from spherical microcavities" has been explained using the geometric optics point of view as well as the classical electrodynamics and quantum theory. The methods for excitation of resonances and analysis for coupling parameters are demonstrated.

The next chapter considers MDR's as transducing mechanisms. Shift and tuning of MDR's with currently known mechanisms are presented. These mechanisms are reviewed and analyzed thoroughly for the understanding and developing a rather new mechanism with liquid crystals. The structural, chemical, optical, and electro-optical properties of liquid crystals and the idea to use the properties of liquid crystals with high Q factor optical resonances of spherical cavities are the main focus of this chapter.

In chapter 4, experimental setup, properties of instruments and the principle of operation of the experimental setup are described. Then the experimental observation of MDR's of spherical microcavities is presented. Later, MDR's are investigated for the changes of their features in water and ethylene glycol. Finally, the MDR's of a silicon microsphere are shifted electro-optically by making use of nematic liquid crystals. Also, electro-optical modulation with MDR's of a silicon microsphere in a liquid crystal has been shown.

Despite the primal operation and applications of optically resonant spherical cavity-liquid crystal systems, orientation control and high refractive index waveguide coupling to high refractive index glass microspheres is essential for the future experiments. Orientation control of liquid crystals could reduce the scattering losses due to liquid crystal molecules. High refractive index waveguide coupling could serve for efficient excitation of MDR's. Then the use of high refractive index glass microspheres could help to discern the transducing mechanism, such as thermo-optic or electro-optic.

VITA

Huzeyfe Yılmaz was born in Van, Turkey in 1985. He completed his high school in Özel Burç Lisesi, İstanbul, Turkey in 2003.

He received his B. Sc. degree in Physics from Bilkent University in Ankara, Turkey, in 2009. He worked on ‘Raman and PL Spectroscopy of Quantum Well Structures’’ at Bilkent University Advanced Research Laboratory as his undergraduate thesis with Prof. Atilla Aydınlı.

He then joined the M.Sc. program in Physics at Koç University in Istanbul, Turkey in 2009, as a teaching/research assistant during which, he worked on “Elastic Light Scattering from Glass and Silicon Microspheres in Organic and Crystalline Liquids and in Aqueous Solutions” with Prof. Ali Serpengüzel at Koç University Microphotonics Research Laboratory.

As of fall 2011, he plans to continue his Ph.D. work with Prof. Lan Yang at Washington University Micro/Nano Photonics Laboratory in St. Louis, Missouri, USA.

BIBLIOGRAPHY

[1] H. Kawamoto, "The History of the Liquid Crystal Displays," Proc. IEEE **90**, 490 (2002).

[2] A. Serpengüzel, S. Arnold, and G. Griffel, "Excitation of Resonances of Microspheres on an Optical Fiber," Opt. Lett. **20**, 654 (1995).

[3] A. Watson, "Optical Circuits Turn a Corner," Science **282** 5387 (1998).

[4] R. K. Chang and A. J. Campillo, "Optical Processes in Microcavities," World Scientific, Singapore (1996).

[5] G. Mie, "Beitrage zur Optik truber Medien, speziell kolloidaler Metallosungen," Ann. Phys. Vierte Folge **25**, 377 (1908).

[6] H. Mabuchi and A. C. Doherty, "Cavity Quantum Electrodynamics: Coherence in context," Science **298**, 1372 (2002).

[7] Y. Hibino, T. Maruno and K. Okamoto, "Recent Progress on Large-Scale PLC Technologies with Advanced Functions," NTT Rev. **13**, 4 (2001).

[8] P. Rabei, W. H. Steier, C. Zhang and L. R. Dalton, "Polymer Micro-Ring Filters and Modulators," J. Lightwave Technol. **20**, 1968 (2002).

[9] K. Djordjev, S. J. Choi and P. D. Dapkus, "Microdisk Tunable Resonant Filters and Switches," IEEE Photon. Technol. Lett. **14**, 828 (2002).

[10] K. J. Vahala, "Optical Microcavities," Nature **424,** 839 (2003).

[11] A. Chiasera, Y. Dumeige, P. Feron, M. Ferrari, Y. Jestin, G. N. Conti, S. Pelli, S. Soria and G. C. Righini, "Spherical Whispering-Gallery-Mode Microresonators," Laser Photon. Rev. **4,** 457 (2010).

[12] F. Vollmer and S. Arnold, "Whispering-Gallery-Mode Biosensing: Label-Free Detection Down to Single Molecules," Nature Methods **5**, 591 (2008).

[13] M. Kerker, “The Scattering of Light and Other Electromagnetic Radiation,” Academic Press, New York (1969).

[14] H. C. van de Hulst, “Light Scattering by Small Particles,” Dover, New York (1981).

[15] C. F. Bohren and D. R. Huffman, “Absorption and Scattering of Light by Small Particles,” Interscience, New York (1983).

[16] R. K. Chang and P. W. Barber, “Optical Effects Associated with Small Particles,” World Scientific, Singapore (1988).

[17] H. M. Nussenzweig, “Diffraction Effects in Semiclassical Scattering,” Cambridge University Press, New York (1992).

[18] B. R. Johnson, “Theory of morphology-dependent resonances: shape resonances and width formulas,” J. Opt. Soc. Am. A **10**, 343 (1993).

[19] J. H. Harlow, “Electric Power Transformer Engineering,” CRC Press LLC, Boca Raton (2004).

[20] M. H. Tooley, “Electronic Circuits: Fundamentals and Applications,” Newnes, Oxford (2006).

[21] D. Kajfez and P. Guillon, “Dielectric Resonators,” Noble Publishing Corp, Atlanta (1998).

[22] H. A. Haus, “Waves and Fields in Optoelectronics,” Prentice-Hall, New Jersey (1984).

[23] L. Weinstein, “Open Resonators and Open Waveguides,” The Golem Press, Boulder (1969).

[24] M. L. Gorodetsky, A. A. Savchenkov and V. S. Ilchenko, “Ultimate Q of Microsphere Resonators,” Opt. Lett. **21**, 453 (1996).

[25] K. H. Guenther and P. G. Wierer, “Surface Roughness Assessment of Ultra Smooth Mirrors and Substrates,” Proc. SPIE, **401**, 266 (1983).

[26] K. J. Vahala, “Optical Microcavities,” World Scientific, Singapore (2004).

[27] P. Chýlek, J. T. Kiehl, and M. K. W. Ko, "Narrow resonance structure in the Mie scattering characteristics," Appl. Opt. **17**, 3019 (1978).

[28] P. Chýlek, "Resonance Structure of Mie Scattering: Distance between Resonances," J. Opt. Soc. Am. A **17,** 1609 (1990).

[29] S. M. Spillane, T. J. Kippenberg, O. J. Painter, and K. J. Vahala, "Ideality in a Fiber Taper-Coupled Microresonator System for Application to Cavity Quantum Electrodynamics," Phys. Rev. Lett. **91,** 043902 (2003).

[30] G. Griffel, S. Arnold, D. Taşkent, and A. Serpengüzel, "Morphology dependent resonances of a microsphere-optical fiber system," Opt. Lett. **21,** 695 (1996).

[31] M. L. Gorodetsky and V. S. Ilchenko, "Optical microsphere resonators: optimal coupling to high-*Q* whispering-gallery modes," J. Opt. Soc. Am. B **16**, 147 (1999).

[32] A. Serpengüzel, S. Arnold, and G. Griffel, and J. A. Lock, "Enhanced Coupling to Microsphere Resonances with Optical Fibers," J. Opt. Soc. Am. B **14**, 790 (1997).

[33] M. Cai and K. J. Vahala, "Highly efficient hybrid fiber taper coupled microsphere laser," Opt. Lett. **26**, 884 (2001).

[34] J. C. Knight, G. Cheung, F. Jacques, and T. A. Birks, "Phase-matched excitation of whispering-gallery-mode resonances by a fiber taper," Opt. Lett. **22**, 1129 (1997).

[35] Y. Panitchob, G. Murugan, Senthil, M. N. Zervas, P. Horak, S. Berneschi, S. Pelli, G. Nunzi Conti, and J. S. Wilkinson, "Whispering gallery mode spectra of channel waveguide coupled Microspheres," Opt. Express, **16**, 11066 (2008).

[36] M. L. Gorodetsky and V. S. Ilchenko, "High-Q optical whispering-gallery microresonators: precession approach for spherical mode analysis and emission patterns with prism couplers," Opt. Commun. **113**, 133 (1994).

[37] S. M. Spillane, T. J. Kippenberg, O. J. Painter, and K. J. Vahala "Ideality in a Fiber-Taper-Coupled Microresonator System for Application to Cavity Quantum Electrodynamics" Phys. Rev. Lett. **91**, 723 (2003).

[38] S. M. Weiss, M. Molinari, and P. M. Fauchet, "Temperature stability for silicon-based photonic band-gap structures," Appl. Phys. Lett. **83**, 1980 (2003).

[39] L. He, Y. F. Xiao, J. Zhu, S. K. Özdemir and L. Yang, "Oscillatory thermal dynamics in high-Q PDMS-coated silica toroidal microresonators," Opt. Express **17**, 9571 (2009).

[40] T. Carmon, L. Yang, and K. J. Vahala, "Dynamical thermal behavior and thermal self-stability of microcavities," Opt. Express **12**, 4742 (2004).

[41] A. M. Armani, R. P. Kulkarni, S. E. Fraser, R. C. Flagan, and K. J. Vahala, "Label-free, single-molecule detection with optical microcavities," Science **317**, 783 (2007).

[42] R.A. Soref and B.A. Bennett, ''Electrooptical effects in Silicon,'' IEEE J. Quantum Electron. **23**, 123 (1987).

[43] F. Vollmer, D. Braun, A. Libchaber, M. Khoshsima, I. Teraoka, and S. Arnold, "Protein Detection by Optical Shift of a Resonant Microcavity," Appl. Phys. Lett. **80**, 4057 (2002).

[44] A. M. Armani, D. K. Armani, B. Min, K. J. Vahala, and S. M. Spillane, "Ultra-high-Q microcavity operation in H20 and D20," Appl. Phys. Lett. **87**, 151118 (2005).

[45] A. Serpengüzel, A. Kurt, and U.K. Ayaz, "Silicon microspheres for electronic and photonic integration," Photon. Nanostructur. Fundam. Appl. **6**, 179 (2008).

[46] V. S. Ilchenko, A. A. Savchenkov, J. Byrd, I. Solomatine, A. B. Matsko, D. Seidel, and L. Maleki, "Crystal quartz optical whispering-gallery resonators**,"** Opt. Lett. **33**, 1569 (2008).

[47] A. Yariv, "Optical Electronics in Modern Communications," Oxford University Press, New York (1997).

[48] G. T. Reed and A. P. Knights, "Silicon Photonics," Wiley, Cornwall (2004).

[49] E. Yüce, O. Gürlü, and A. Serpengüzel, "Optical Modulation with Silicon Microspheres," IEEE Photon. Technol. Lett., **21**, 1481 (2009).

[50] G. Gilardi, D. Donisi, A. Serpengüzel, and R. Beccherelli, "Liquid-crystal tunable filter based on sapphire microspheres," Opt. Lett. **34**, 3253 (2009).

[51] E. Lueder, "Liquid Crystal Displays: Addressing Schemes and Electro-Optical Effects," Wiley, West Sussex (2001).

[52] P. Yeh and C. Gu, "Optics of Liquid Crystal Displays," Wiley, New York (1999).

[53] S. Chandrasekhar, "Liquid Crystals," Cambridge Univ. Press, Cambridge (1977).

[54] P. G. de Gennes, "The Physics of Liquid Crystals," Clarendon Press, Oxford (1974).

[55] L. Jun, W. Chien-Hui, S. Gauza, R. Lu and W. Shin-Tson, "Refractive Indices of Liquid Crystals for Display Applications," J. Disp. Technol. **1**, 51 (2005).

[56] L. M. Blinov and V. G. Chigrinov, "Electrooptic effects in liquid crystal materials," Springer-Verlag (1994).

[57] M. Humar, M. Ravnik, S. Pajk and I. Musevic, "Electrically tunable liquid crystal optical microresonators," Nature Photon. **3**, 595 (2009).